

Synthesis of a Novel Photothermal Polymer for Use in Gas Hydrate Inhibition

Thomas Vlastic
Department of Chemical Engineering
McGill University
Montreal, Quebec, Canada
April, 2014

A thesis submitted to McGill University in partial
fulfillment of the requirements of the degree of
Master of Chemical Engineering

©Copyright Thomas Vlastic, 2014



Table of Contents

1.0	Introduction.....	1
2.0	Objectives	3
3.0	Literature Review.....	4
3.1	Gas hydrate phase equilibrium.....	4
3.2	Conductive polymers.....	5
3.2.1	Background.....	5
3.2.2	Band theory (metals, semiconductors and insulators)	7
3.2.3	Conduction mechanism.....	10
3.2.4	The photothermal behaviour of conducting polymers	13
4.0	Materials and Methods.....	14
4.1	Synthesis of poly(3-hexylthiophene)-b-poly(ethylene oxide).....	14
4.1.1	Synthesis of regioselective poly(3-hexylthiophene).....	14
4.1.2	Synthesis of borolane mono-end-capped poly(ethylene oxide) (PEO-BE)	15
4.1.3	Synthesis of poly(3-hexylthiophene)-b-poly(ethylene oxide) diblock copolymer .	16
4.2	Photothermal Testing	17
4.2.1	Initial experiments	17
4.2.2	Cold plate experiments	18
4.2.3	IR camera experiments	20
4.2.4	Final experiments.....	20
5.0	Results.....	22
5.1	Characterization of poly(3-hexylthiophene)	22
5.2	Photothermal testing.....	26
5.2.1	Initial experiments	26
5.2.2	Cold plate experiments	26
5.2.3	IR camera experiments	30
5.2.4	Final experiments.....	31
6.0	Discussion.....	33
7.0	Conclusion	37
7.1	Recommendations	38
8.0	References.....	39
	Appendix.....	41
A-1	Characterization of P3HT synthesized using 5% nickel catalyst.....	41

List of Figures

Figure 1. Methane-water phase diagram.....	4
Figure 2. Examples of conjugated polymers.....	6
Figure 3. The bands and band gap of different types of materials around the Fermi level.	8
Figure 4. Typical band structure of an insulating material.	9
Figure 5. Bipolaron formation in a conducting polymer upon doping.	11
Figure 6. Polyacetylene's two energetically identical structures (a, b), and polythiophene's aromatic-like ground state (c) and higher energy quinoid-like structure (d).	12
Figure 7. Soliton formation in polyacetylene upon doping.	13
Figure 8. The synthesis pathway for P3HT.	15
Figure 9. The synthesis pathway for PEO-BE.	16
Figure 10. The synthesis pathway for P3HT- <i>b</i> -PEO.	17
Figure 11. Initial experiments diagram.	18
Figure 12. KL 2500 LCD light source emission spectrum.	18
Figure 13. Diagram of the cooling plate setup.....	19
Figure 14. Diagram of the IR camera setup.	20
Figure 15. KL 2500 LED light source emission spectrum.	21
Figure 16. The ¹ H NMR spectrum of P3HT.	22
Figure 17. UV-vis absorption spectra of P3HT in THF synthesized using 5% of Ni catalyst.	23
Figure 18. MALDI-TOF mass spectrum of hexane fraction of P3HT synthesized using 2% Ni catalyst and used for P3HT-PEO synthesis.	24
Figure 19. GPC (THF, against polystyrene standard) of the lower molecular weight P3HT extracted with hexane, synthesized using 2% Ni catalyst and used for P3HT-PEO synthesis.....	25
Figure 20. GPC (THF, against polystyrene standard) of the higher molecular weight P3HT extracted with chloroform and synthesized using 2% Ni catalyst.	25
Figure 21. Temperature as a function of time of 1 mL of the three samples in a plastic cuvette exposed to the LCD light source, starting at room temperature.	26
Figure 22. Temperature as a function of time of 2 mL of the three samples in the metal cuvette on the cooling plate exposed to the LCD light source, starting from room temperature.....	27
Figure 23. Temperature as a function of time of 2 mL of the three samples in the metal cuvette on the cooling plate set to -15°C starting from room temperature (20°C).	28
Figure 24. Temperature as a function of time of 2 mL of the three samples exposed to the LCD light source after being frozen in the metal cuvette while the cooling plate was set to -15°C.	29
Figure 25. Temperature as a function of time of 2 mL of the three samples in the metal cuvette exposed to the LCD light source while the cooling plate is set at -15°C starting from room temperature.	30
Figure 26. Temperature (measured with an IR camera) as a function of time of 1 mL of the three samples previously frozen in a plastic cuvette and exposed to the LCD light source.	31

Figure 27. Temperature as a function of time of 1 mL of sample in a transparent plastic cuvette exposed to the LED light source, starting from room temperature..... 32

Abstract

One of the most significant challenges in the transportation of natural gas is the potential for gas hydrates to cause pipeline blockages. One way of ensuring the inhibition of gas hydrates is simply by maintaining the system temperature above the hydrate equilibrium temperature. Low-concentration aqueous solutions of certain inorganic nanoparticles have been shown to generate significant amounts of heat when subjected to a laser of a certain wavelength. This photothermal effect could be sufficient to thermodynamically inhibit hydrate formation. However, these inorganic nanoparticles are often not biodegradable or potentially harmful to the environment.

Therefore, a non-toxic water-soluble block copolymer, poly-3-hexylthiophene-*b*-polyethylene oxide (P3HT-PEO), was synthesized as a possible hydrate inhibitor. Its photothermal potential was assessed, and compared to poly(3,4-ethylenedioxythiophene):polystyrene sulfonate (PEDOT:PSS), a known photothermal polymer, using water as a control. Low concentration aqueous solutions of these two polymers were subjected to a light source in order to determine whether the presence of the polymers increased the temperature of water, melted ice more quickly and prevented the water from freezing under a constant cooling load.

It was found that both polymer solutions had a photothermal effect, increasing in temperature by 4-10°C after five minutes of light exposure, while water showed no increase. Furthermore, it was observed that half of the frozen P3HT-PEO sample melted after 45 minutes of exposure to the light source under constant cooling load (-15°C), while the PEDOT:PSS sample melted only near the top, and the ice remained completely frozen. Also, the two frozen polymer samples melted much more quickly than ice when exposed to the light source at room temperature. However, it was unable to be determined whether the presence of these polymers could prevent the water from freezing upon exposure to the light source under a constant cooling load. Finally, it was found that water with dark food colouring increased just as much in temperature as the P3HT-PEO solution of the same colour when exposed to the light source.

Abrégé

Un problème majeur dans le transport du gaz naturel est la possibilité de formation d'hydrates de gaz qui peuvent causer des blocages de gazoducs. Une manière d'assurer l'inhibition des hydrates de gaz est simplement de maintenir la température du système plus haut que la température d'équilibre thermodynamique entre le gaz, le liquide et les hydrates. Il a été démontré que des solutions aqueuses à faible concentration de certaines nanoparticules inorganiques produisent de la chaleur lorsqu'ils sont soumis à un laser d'une certaine longueur d'onde. Cet effet photothermique pourrait être suffisant pour thermodynamiquement prévenir la formation des hydrates. Cependant, souvent ces nanoparticules inorganiques ne sont pas biodégradables ou sont potentiellement nocifs pour l'environnement.

Conséquemment, un copolymère séquencé non-toxique et soluble dans l'eau, poly(3-hexylthiophène)-b-poly(oxyde d'éthylène) (P3HT-PEO), a été synthétisé comme un inhibiteur possible d'hydrates. Son potentiel photothermique a été évalué et comparé à poly(3,4-éthylènedioxythiophène): polystyrène sulfonate (PEDOT: PSS), un polymère photothermique connu, en utilisant de l'eau comme expérience témoin. Des solutions aqueuses à faible concentration de ces deux polymères ont été exposées à une source de lumière afin de déterminer si la présence des polymères augmenterait la température de l'eau, fondrait la glace plus rapidement, et empêcherait l'eau de geler sous une charge de refroidissement constante.

Il a été trouvé que les deux solutions de polymère ont un effet photothermique, augmentant en température par 4-10°C après cinq minutes d'exposition à la lumière, tandis que l'eau n'a pas augmenté en température. De plus, il a été observé que la moitié du P3HT-PEO congelé a fondu après 45 minutes d'exposition à la source de lumière sous une charge constante de refroidissement (-15 ° C), tandis que le PEDOT: PSS a fondu seulement vers le haut, et la glace a resté complètement gelé. Aussi, les deux solutions de polymères congelées ont fondu beaucoup plus rapidement que la glace lorsqu'elles ont été exposées à la lumière, à température ambiante. Cependant, il n'a pas pu être déterminé si la présence de ces polymères pourrait empêcher l'eau de geler lors de leur exposition à la lumière sous une charge de refroidissement constante. Enfin, il a été trouvé que l'eau avec du colorant alimentaire foncé a augmenté autant en température que la solution de P3HT-PEO de la même couleur lorsqu'elles ont été exposées à la source de lumière.

Acknowledgements

First and foremost, I would like to thank my supervisors Dr. Phillip Servio and Dr. Milan Maric for their advice and guidance throughout the course of my research.

I would also like to thank Chi Zhang for the many hours spent training me in polymer synthesis techniques, Iryna Perepichka for helping me with all of the polymer synthesis, Jason Ivall for setting up the cooling plate, metal cuvettes and thermocouples, Edwin Ling for writing the LabVIEW program which was used to operate the cooling plate and Roya Jamarani for all of her help editing my thesis. Thank you to the rest of my laboratory group as well for their help and support.

This research was funded by the Eugenie Ulmer Lamothe Scholarship.

1.0 Introduction

In the last decade, the vast deposits of methane in the form of gas hydrates occurring naturally below the permafrost zone and in sub-sea sediments are increasingly being considered as a potential alternative energy source to reduce the current economy's reliance on oil and coal [1]. However, efficiently extracting these deposits at such great depths has proven to be a considerable challenge. These hydrates form under high pressure and low temperature and remain thermodynamically stable under these conditions. Consequently, problems can arise during the transportation of natural gas in pipelines where conditions can be favourable for the formation of gas hydrates, potentially leading to pipeline blockages. Various methods to prevent the formation of gas hydrates exist, such as using thermodynamic inhibitors (methanol, glycol) or kinetic inhibitors, which have been reported to have varying degrees of success [2]. On the one hand, thermodynamic inhibitors are required in large volumes in order to be effective and are often very difficult to recuperate while being toxic to the environment. On the other hand, although kinetic inhibitors, also known as low dosage hydrate inhibitors (LDHI), are used in low concentrations, their research and development is expensive, and they are not effective enough to be used industrially.

One way of ensuring the inhibition of gas hydrates is simply by keeping the temperature of the vapor-liquid mixture above the liquid-hydrate-vapor equilibrium temperature. Unfortunately, the use of heaters or hot water is economically and practically unfeasible, and a more targeted approach, which has been observed with LDHIs, is preferable. One method that may encompass the advantages of heaters and LDHIs is a photothermal approach. The principle behind this method is that when certain nanoparticles (gold, carbon nanotubes, graphene, copper

selenide, porous silicon, among others) are subjected to a laser of a certain wavelength, they absorb the photons and generate heat due to the surface plasmon resonance (SPR). Aqueous solutions containing very low concentrations of these nanoparticles have been reported to produce significant heating (up to 30°C) upon laser irradiation ($<1\text{W}/\text{cm}^2$) in just a few minutes [3-6]. Therefore, these nanoparticles in solution could in theory constantly generate heat in order to keep the temperature of the methane-water mixture above the hydrate formation temperature (at a given pressure). However, these nanoparticles are often inorganic compounds which are either not biodegradable or potentially harmful to the environment. Therefore, there is a further need to develop a similar system which does not require the use of these inorganic nanoparticles, but rather a polymer nanoparticle capable of the same photothermal effect.

The focus of this project is to examine the effect of light absorption on aqueous polymer solutions of low concentration in order to inhibit the formation of hydrates. A novel, non-toxic, water-soluble, photothermal block copolymer poly(3-hexylthiophene)-*b*-polyethylene oxide (P3HT-PEO) will be synthesized. Its photothermal and hydrate inhibiting potential will be assessed, and compared to the proven photothermal polymer mixture poly(3,4-ethylenedioxythiophene):polystyrene sulfonate (PEDOT:PSS) [7].

2.0 Objectives

One of the primary goals of my research was to synthesize and characterize a novel water-soluble block copolymer capable of exhibiting photothermal behaviour. It was expected that small amounts of this polymer (10 mg/mL or less) dissolved in water would generate heat when exposed to a laser or light source, thereby increasing the temperature of the solution. Most of the research to date regarding photothermal polymers has dealt either with conductive nanoparticles coated with a water soluble polymer or with a mixture of two ionomers, such as PEDOT:PSS, with one ionomer being conductive and the other being water soluble. It was desirable to synthesize a block copolymer since it has the interesting ability to form micelles when dissolved in solution. These micellar molecules could prove to be more effective in photothermal conversion or even in the disruption of hydrate growth than their nanoparticle counterparts.

The second goal of my research was to characterize the effect of this novel photothermal polymer on water temperature and on the freezing and melting of ice. Experiments studying the effect of this block copolymer on water and ice in the presence of light are the first step in determining whether photothermal polymers are suitable for use as hydrate inhibitors, since gas hydrates have a similar structure to ice. The temperature increase of the aqueous polymer solution after exposure to light was compared to the temperature increase of water, as a control, as well as to an aqueous solution of PEDOT:PSS, a conjugated polymer mixture proven to exhibit a photothermal effect [7].

3.0 Literature Review

3.1 Gas hydrate phase equilibrium

The principle behind hydrate inhibition using light absorption by a dilute aqueous solution of a photothermal polymer can be explained by the methane-water phase diagram, shown in Figure 1 below. Figure 1 is an example of a phase diagram of a typical hydrate forming system.

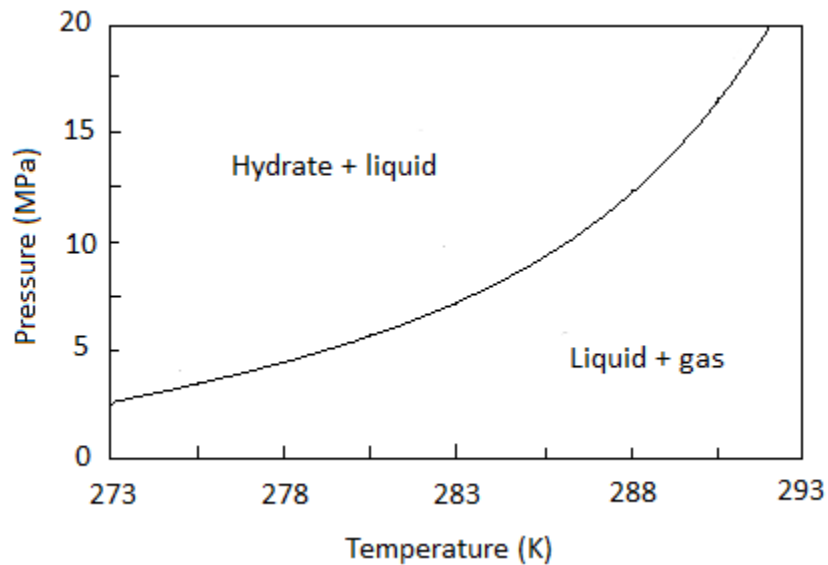


Figure 1. Methane-water phase diagram.

The curve represents the three-phase equilibrium state between liquid water, methane vapor and methane hydrates. Above this three phase equilibrium line, the two phases present are methane hydrates and either liquid water or methane vapor (depending on the limiting phase), while below the equilibrium line, the two phases present are liquid water and methane vapor, and hydrate formation is thermodynamically impossible [1]. Therefore, at a given pressure, it is

desirable to increase the temperature in order to move beneath the equilibrium line where no methane hydrates can form [9]. Theoretically, this could be achieved by adding a dilute amount of a soluble photothermal polymer to a methane-water system under favourable hydrate-forming conditions, and exposing this system to a light source.

Thermodynamic inhibitors prevent the formation of gas hydrates by shifting the hydrate-liquid-vapour equilibrium curve to the left in Figure 1, towards higher pressures and lower temperatures. Kinetic inhibitors, however, delay the onset of nucleation, which increases the time required for hydrate formation. Unlike thermodynamic or kinetic inhibitors, the method involving photothermal polymers does not alter the activity of the solution or the kinetics of hydrate formation; it simply ensures that the temperature conditions are such that hydrate nucleation and growth become thermodynamically impossible. This technology has the potential advantage of drastically increasing heat at low chemical concentrations [9].

3.2 *Conductive polymers*

3.2.1 Background

Until the 1960's, polymers were considered first and foremost as electrical and thermal insulators, and were used almost solely for this purpose [10]. However, in 1958, polyacetylene, the first conducting polymer, was synthesized by Natta et al. which sparked a significant increase in interest and research in the field of conducting polymers [10]. Materials can be classified as conductors (metals), semiconductors or insulators, depending on how well they conduct electricity. Polyacetylene has such a high conductivity that it falls into the category of metals

[10]. All other conducting polymers synthesized thereafter fall into the category of semiconductors, characterized by having an electrical conductivity between that of a conductor and an insulator [10, 11].

Conducting polymers can also be referred to as conjugated polymers as they all consist of alternating single and double bonds in their backbone. Figure 2 illustrates some of the most common examples of conjugated and hence conductive polymers.

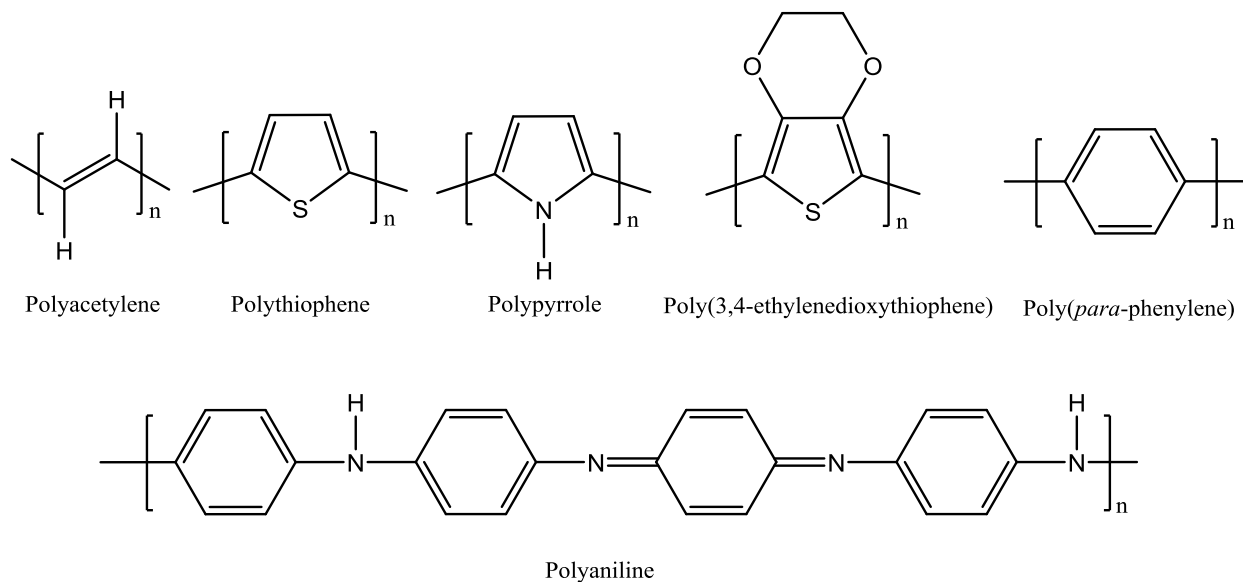


Figure 2. Examples of conjugated polymers.

Conducting polymers can conduct electricity due to their conjugated backbone. The alternating single and double bonds allow electrons to delocalize along the polymer chain and to be shared by many atoms. The delocalized electrons can then move up and down the polymer chain essentially becoming the charge carriers that make the polymer conductive. The first conjugated polymers synthesized were not intrinsically electrically conductive, and most today are still not. However, they can be transformed into their conductive state by adding or removing

electrons from the polymer backbone creating cations or anions, respectively [10]. This process is called doping. It allows electrons to flow due to the formation of “conduction bands”.

Likewise, a polymer’s conductive potential has a lot to do with how easily electrons can be added or removed from the system [12]. The double bonds of unsaturated polymers like conjugated polymers consist of a strong σ bond as well as a weaker π bond. The electrons found in the π bonds can be added or removed relatively easily, making unsaturated polymers potentially much more conductive than their saturated counterparts which only have sigma bonds [12].

3.2.2 *Band theory (metals, semiconductors and insulators)*

A solid material has an infinite number of bands in its electronic structure separated by band gaps. However, most of these bands are either too high in energy or too low in energy to be significant. The high energy bands never get filled by electrons, and the low energy bands, associated with the core orbitals, always remain filled [11]. The most important bands and band gaps are located in and around the Fermi level, E_F [13]. In semiconductors and insulators, the conduction band is the first band above the Fermi level, while the valence band is the first band below [14]. These two bands are separated by a band gap. In metals however, the Fermi level is located inside the overlapping valence and conduction bands since there is no band gap as seen in Figure 3 [11, 14].

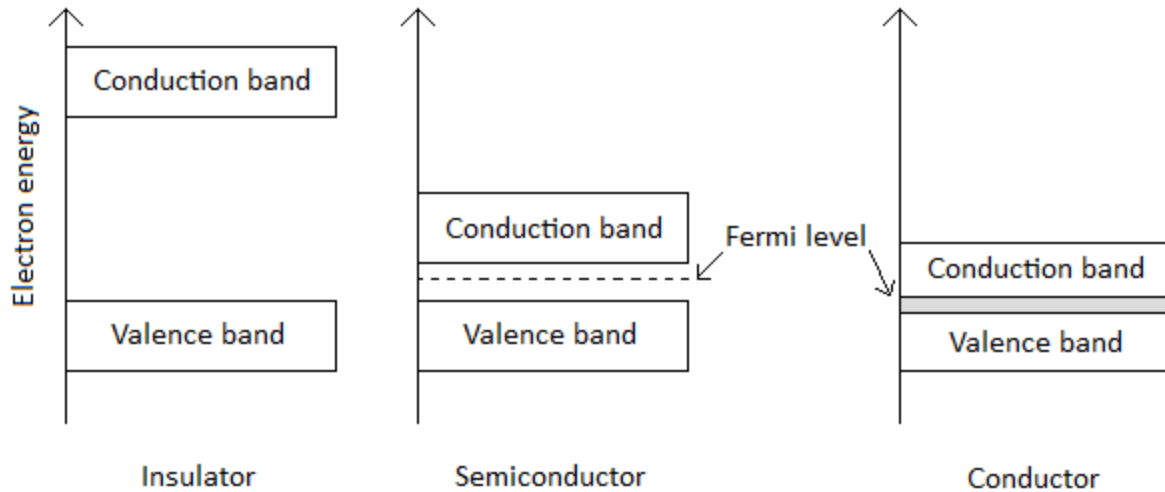


Figure 3. The bands and band gap of different types of materials around the Fermi level.

As previously mentioned, the conduction band is located right above the valence band on a graph of the electronic structure of a material, as seen in Figure 4 [16]. The valence band is where electrons with the highest amount of energy still bound to the atom are found [17]. Electrons in the conduction band however have enough energy to free themselves from the atom to which they are bound and are able to move around as delocalized electrons [13]. These electrons are mobile charge carriers responsible for electrical conductivity [16]. There is a band gap between the valence band and the conduction band which an electron must jump in order to become a free electron [17]. No electron can exist at an energy level located inside the band gap [16]. This band gap represents the minimum amount of energy required for an electron to move from the lower band to the higher band. Therefore, the size of the band gap is a major factor in determining the electrical conductivity of a material.

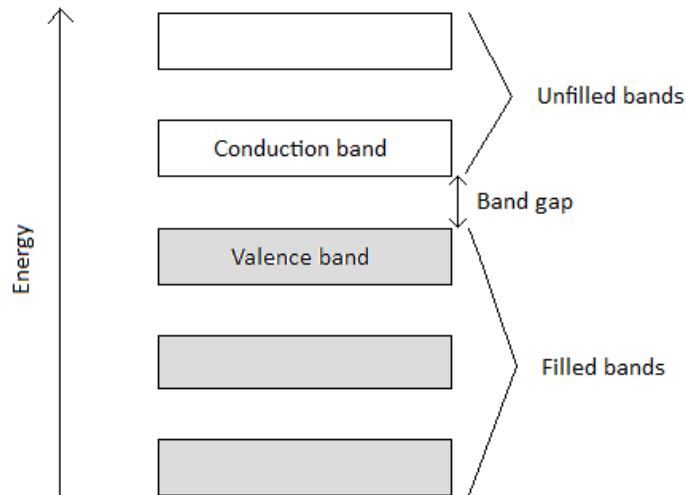


Figure 4. Typical band structure of an insulating material.

For insulators, this band gap is large, and the energy required to jump from the valence band to the conduction band is too high [17]. Consequently, the electrons are unable to delocalize, making the material unable to conduct electricity. Semiconductors have a small band gap, and therefore require little energy to delocalize electrons [17]. This energy can come in the form of heat or light (phonon or photon) [15]. This is why the conductivity of semiconductors increases with temperature [13, 17]. Conductors, however, often do not have a band gap; the valence band and the conduction band overlap as seen in Figure 3 [11, 17]. Therefore, no energy is required for the valence electrons to become conduction electrons which then become mobile charge carriers.

Upon exposure to light, a semiconductor may absorb enough energy for some of its valence electrons to become free and no longer bound to a single atom, leaving electron holes as they move from the valence band to the conduction band [18]. Both the mobile electrons and the holes they create contribute to the electrical conductivity of the material. This phenomenon is called photoconductivity, whereby the conductivity of a material (in most cases semiconductors)

increases upon absorption of electromagnetic radiation such as visible light, an important phenomenon related to the photothermal behaviour of certain polymers [18].

3.2.3 *Conduction mechanism*

It was previously thought that conducting polymers owed their conductivity to unfilled electronic bands, much like the mechanisms described above [10, 12]. Oxidization would remove electrons from the top of the valence band, creating electron holes, and reduction would add them to the bottom of the conduction band, creating conduction electrons [19]. However, it was soon discovered that unpaired electrons were not responsible for the conductivity of these polymers, unlike most conventional semiconductors [12]. The charge carriers were in fact bipolarons or solitons, which are charges associated with local distortions in the lattice. For example, upon oxidation, a conducting polymer could either lose an electron (from the valence band) or localize the charge over a small portion of the chain [10]. The change in geometry to a quinoid-like structure, as seen in Figure 5, due to the charge localization is more energetically favourable than charge delocalization [10]. Therefore, a polaron is formed which consists of a charge site (cation) in combination with a free radical [19]. In this case the valence band remains full and the conduction band remains empty. However, two new localized electronic states are created within the band gap called polaron states, the lower of which becomes half-occupied by an unpaired electron, shown in Figure 5 [10]. When another electron is removed from the polymer chain upon further oxidation, it is more favourable for the electron to be taken from the existing polaron than to form a separate polaron [10, 12]. The free radical then becomes another charge site (cation), and a bipolaron is formed instead of two polarons [10]. The bipolaron is

thermodynamically more stable than two polarons even with the repulsive force created by having two positive charges so close together [12].

The polaron states in the band gap are replaced by bipolarons, and eventually, at high doping levels, the bipolaron states overlap, forming two distinct bipolaron bands, shown in Figure 5 [10]. These two bands can continue broadening until they merge with the valence band and the conduction band, essentially connecting the two bands and creating metallic-like conductivity [10, 12]. The bands are partially filled, and the bipolarons become the mobile charge carriers responsible for the transport of the current, not the electrons [12].

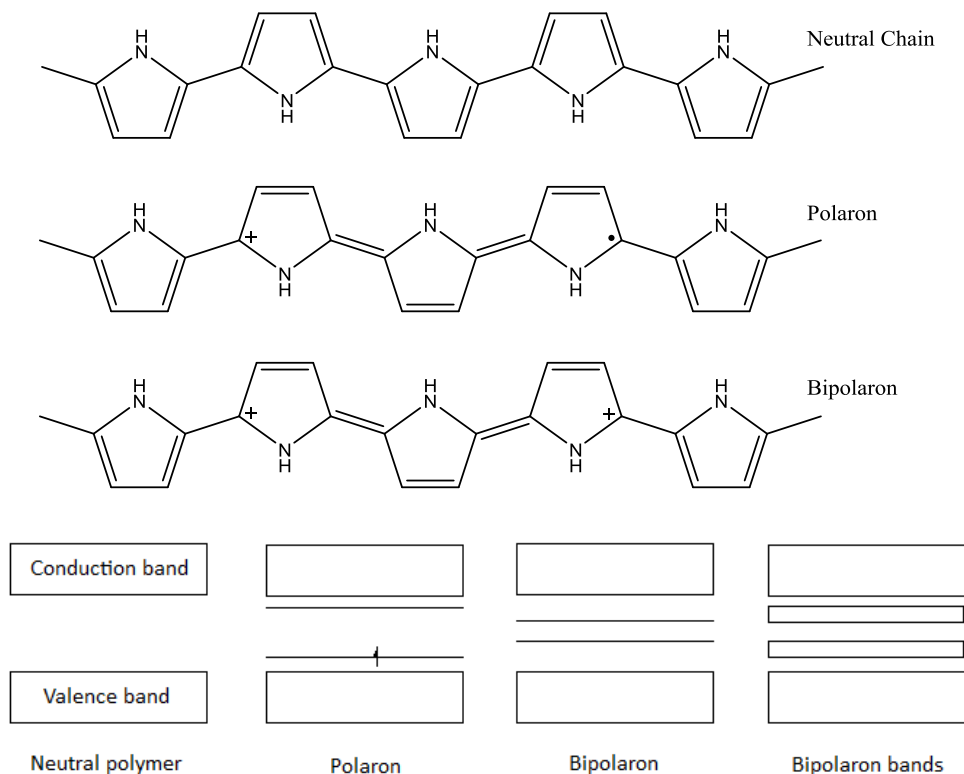


Figure 5. Bipolaron formation in a conducting polymer upon doping.

In polymer systems like poly(*p*-phenylene), polypyrrole and polythiophene, which have a non-degenerate ground state, bipolarons are the main source of charge carriers and are responsible for conduction [19]. In polymer systems like polyacetylene, which have a degenerate

ground state, the charge carriers are not bipolarons, but are called solitons [10]. Polyacetylene is referred to as degenerate because it has two geometric structures that correspond to exactly the same total energy, shown in Figure 6. Although polythiophene, for example, can have two different structures, as seen in Figure 6, the quinoid-like structure is of higher energy, and therefore, the aromatic structure is thermodynamically more favourable as a ground state, which is why it is referred to as non-degenerate [12]. Upon oxidation, however, since the quinoid-like structure has a higher electron affinity, the polymer chain tends to switch configurations [12].

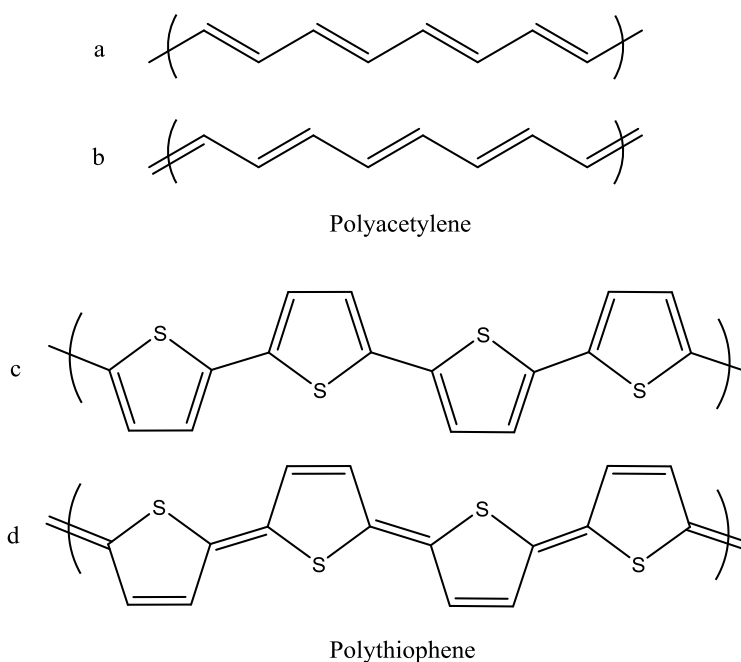


Figure 6. Polyacetylene's two energetically identical structures (a, b), and polythiophene's aromatic-like ground state (c) and higher energy quinoid-like structure (d).

In a system like polyacetylene (with a degenerate ground state), solitons replace bipolarons as the main source of charge carriers [12]. Oxidation of this type of polymer initially leads to the formation of a polaron (a cation and a free radical), but unlike in polymers with a non-degenerate ground state, the polarons are independent of each other and have no energetic incentive to combine and form bipolarons [10, 12]. This results in sections of different

orientations, but of equal energy along the polymer chain each separated by a charged defect (charged cation) which is referred to as a soliton, as seen in Figure 7 [10].

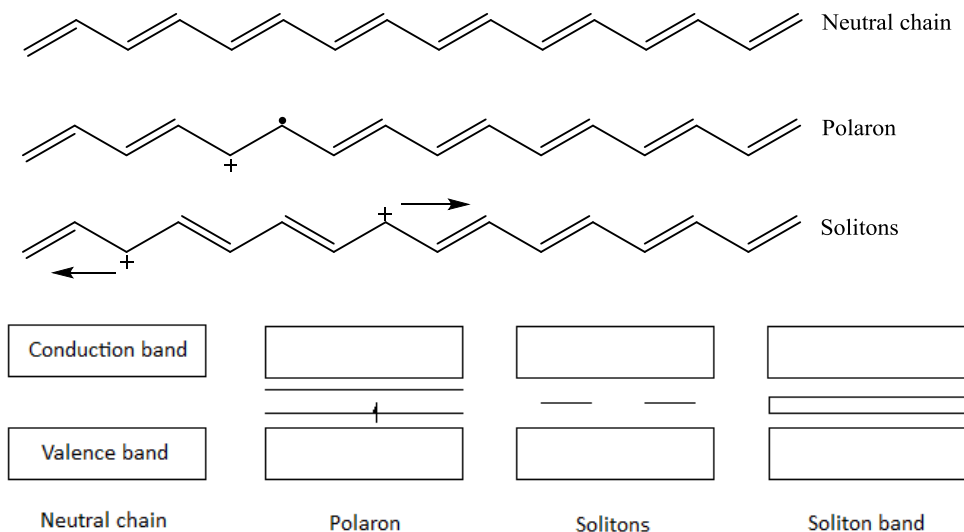


Figure 7. Soliton formation in polyacetylene upon doping.

3.2.4 The photothermal behaviour of conducting polymers

The photothermal behaviour of conducting polymers has not yet been fully understood unlike their metal counterparts. However, it has been hypothesized that upon photoexcitation, polarons are formed within the polymer, similarly to the way a polaron is formed upon oxidation or reduction [20]. As described above, these polarons do not stay as polarons, but tend to form bipolarons or solitons, upon further oxidation or in this case photoexcitation.

Both polarons and bipolarons are associated with distinct local lattice distortions. When two polarons combine to form a bipolaron, the distortion in the lattice changes [21]. This change causes vibrations in the lattice, energy which can be transferred to the bipolaron's surroundings. Therefore, two polarons that collide to form a bipolaron can transfer the excess energy into phonons (heat), which then increases the temperature of its surroundings [21].

4.0 Materials and Methods

4.1 *Synthesis of poly(3-hexylthiophene)-b-poly(ethylene oxide)*

The synthesis of the P3HT-PEO block copolymer was performed in three steps. First a Grignard metathesis reaction was performed in order to obtain the P3HT. Then, the PEO was functionalized to obtain the intermediate, PEO-BE. Finally, the P3HT block was added to the PEO-BE block using the Suzuki coupling method.

4.1.1 *Synthesis of regioselective poly(3-hexylthiophene)*

A Grignard Metathesis (GRIM) reaction was performed to synthesize regioregular, head-to-tail coupled, P3HT similarly to the method developed by the McCullough group, as seen in Figure 8 [22]. The polymerization was carried out in a dry, one liter, one-neck round bottom flask with a stir bar and flushed with nitrogen. 2,5-dibromo-3-hexylthiophene (15.37 g, 47.13 mmol, purchased from Sigma-Aldrich), a 2M solution of butylmagnesium chloride in diethyl ether (24 mL, 48 mmol, purchased from Sigma Aldrich) and anhydrous tetrahydrofuran (THF, 300 mL) purged with nitrogen gas were added to the reaction flask [23].

The reaction mixture was stirred for three hours at 60°C with nitrogen bubbling through the solution, and then allowed to cool to room temperature. The nickel catalyst, Ni(dppp)Cl₂ (0.51 g, 0.94 mmol), was dispersed in 100 mL of anhydrous THF purged with nitrogen and was added to the reaction mixture via cannula. The polymerization of 3-hexylthiophene was performed at room temperature for 45 minutes under pressure of nitrogen. The reaction mixture was then quenched with methanol and stirred for an hour. The P3HT precipitated and was

collected by vacuum filtration, then purified by sequential Soxhlet extractions using methanol, hexane and chloroform. The methanol fraction was discarded as it contained only unreacted monomer. The hexane fraction was collected and concentrated using the rotary evaporator (rotavap) to obtain low molecular weight P3HT ($M_n = 2400$ g/mol by GPC). The chloroform fraction was collected and concentrated using the rotavap to obtain the higher molecular weight P3HT as a black solid (7.21 g, 92% yield, $M_n = 9,900$ by GPC) [23].

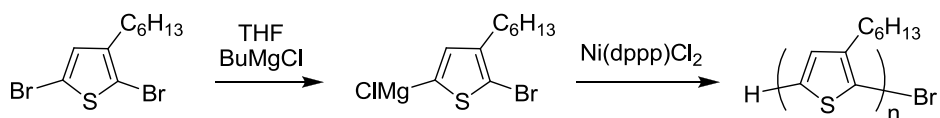


Figure 8. The synthesis pathway for P3HT.

4.1.2 Synthesis of borolane mono-end-capped poly(ethylene oxide) (PEO-BE)

The synthesis of PEO-BE was performed using a method modified from Li et al. [24], illustrated in Figure 9. Poly(ethylene glycol) methyl ether (PEG) (1.01 g, $M_n = 20,000$ g/mol, purchased from Sigma-Aldrich), 4-carboxylphenylboronic acid pinacol ester (0.046 g, 0.185 mmol, purchased from Sigma-Aldrich), N,N-dicyclohexylcarbodiimide (DCC)(0.030 g, 0.145 mmol), N,N-dimethylaminopyridine (DMAP)(0.018 g, 0.147 mmol) and anhydrous THF (75 mL) purged with nitrogen gas were added to a dry 100 mL one-neck round bottom flask flushed with nitrogen gas [23].

The reaction mixture was heated and stirred using a stir bar until all the PEG dissolved. The mixture was then left stirring at room temperature for four days. The solvent was removed using the rotavap, and the remaining product was precipitated (suspended) in diethyl ether. The precipitate was collected by vacuum filtration, then dissolved in approximately 10 mL of

dichloromethane (DCM) and precipitated once more into 125 mL of hexane. The solid was collected by vacuum filtration and washed with diethyl ether to obtain PEO-BE as a white powder (0.98 g) [23].

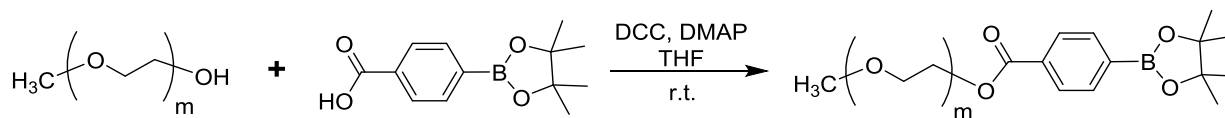


Figure 9. The synthesis pathway for PEO-BE.

4.1.3 Synthesis of poly(3-hexylthiophene)-b-poly(ethylene oxide) diblock copolymer

The block copolymer was synthesized using the Suzuki Coupling method, following a modified version of the procedure described by Li et al. [24], illustrated in Figure 10. The previously synthesized P3HT (0.186 g; $M_n = 2400$ g/mol, $M_w = 2900$ g/mol, $M_w/M_n = 1.20$ by GPC), PEO-BE (0.500 g; $M_n=19500$ g/mol, $M_w=23800$, $M_w/M_n=1.22$), tetrakis(triphenylphosphine)palladium(0) ($\text{Pd}(\text{PPh}_3)_4$) (0.011 g, 0.010 mmol), a 0.406 M solution of K_2CO_3 in H_2O (5 mL) and anhydrous 1,4-dioxane (40 mL) purged with nitrogen were added to a dry one-neck round bottom flask flushed with nitrogen [23].

The reaction mixture was refluxed under nitrogen for four days. It was then diluted with H_2O and added to chloroform to extract the final product. The organic layer was separated and then filtered to remove catalytic residue, followed by concentration using the rotavap. The product was then precipitated into hexane to remove unreacted P3HT. The precipitate was collected by vacuum filtration and dispersed into H_2O to remove unreacted PEO-BE. A vacuum filtration was then performed again to obtain the final product, P3HT-b-PEO, as a red powder (0.315 g) [23].

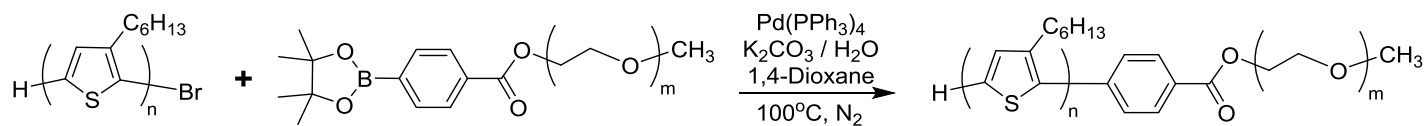


Figure 10. The synthesis pathway for P3HT-*b*-PEO.

4.2 Photothermal Testing

Four sets of experiments were performed to investigate the photothermal behaviour of the polymer samples. Initial experiments were performed in plastic cuvettes to determine whether the polymer solutions exhibited a photothermal effect when exposed to light. Cold plate experiments were performed in metal cuvettes to examine the effect of the polymers on the freezing and melting of water. Infrared (IR) camera experiments were performed in plastic cuvettes to examine the effect of the polymers on the melting rate of ice. Final experiments were performed in plastic cuvettes to investigate the effect of different light sources and solution colour on temperature.

4.2.1 Initial experiments

The initial experiments with the synthesized block copolymer, P3HT-*b*-PEO, were performed in order to assess whether the polymer did indeed have photothermal potential. A 1 mL solution of P3HT-*b*-PEO in water (≈ 10 mg/mL) was put into a transparent plastic cuvette and exposed to a light source (Schott KL 2500 LCD, intensity 4, aperture E) for 20 minutes. The emission spectrum of the LCD light source is shown in Figure 12. Instantaneous temperature

measurements of the solution were obtained using a thermocouple at 5 min, 10 min and 20 min. A diagram of the setup used for these experiments is shown in Figure 11. A solution of PEDOT:PSS (1.3-1.7% solids content, from Ossilla, Heraeus Clevios™ P VP AI 4083) was also tested to compare to the block copolymer. Water was used as a control.

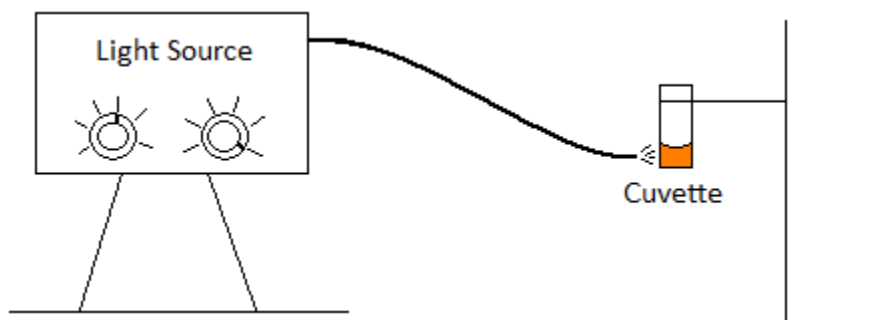


Figure 11. Initial experiments diagram.

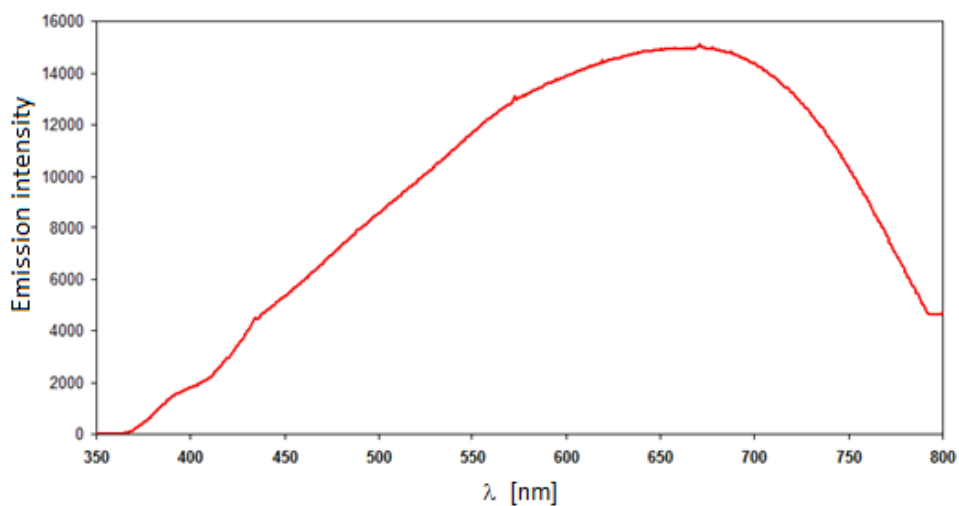


Figure 12. KL 2500 LCD light source emission spectrum.

4.2.2 Cold plate experiments

The next set of experiments was performed using a metal cuvette on a Peltier cooling plate with continuous temperature measurements (one measurement per second). The metal cuvette was made by hollowing out a stainless steel rod (1.25cm in diameter and 2cm in height)

and two thermocouples were inserted into the cuvette, one near the top and one near the bottom. 2 mL of the P3HT-*b*-PEO aqueous solution (10 mg/mL) was put into the cuvette resting on top of the cooling plate. A diagram of the cooling plate setup is shown in Figure 13. Three experiments were performed using this setup. Similar to the initial experiments, the solution in the cuvette was exposed to the light source at room temperature until the solution temperature reached steady state. Then, starting back from room temperature again (20°C), the cooling plate was set to -15°C and the solution was allowed to freeze (with the light source off). Once the solution was frozen and the temperature reached steady state, the light source was turned on and the temperature was recorded until it reached steady state. Lastly, starting from room temperature (20°C), the cooling plate was set to -15°C and at the same time the light source was turned on. The solution was allowed to cool while being exposed to the light, and the temperature was recorded until steady state was reached. These sets of experiments were also performed with PEDOT:PSS as a comparison, and water as a control. These experiments were done in order to determine whether the photothermal effect of the block copolymer was enough to melt ice or to prevent water from freezing.

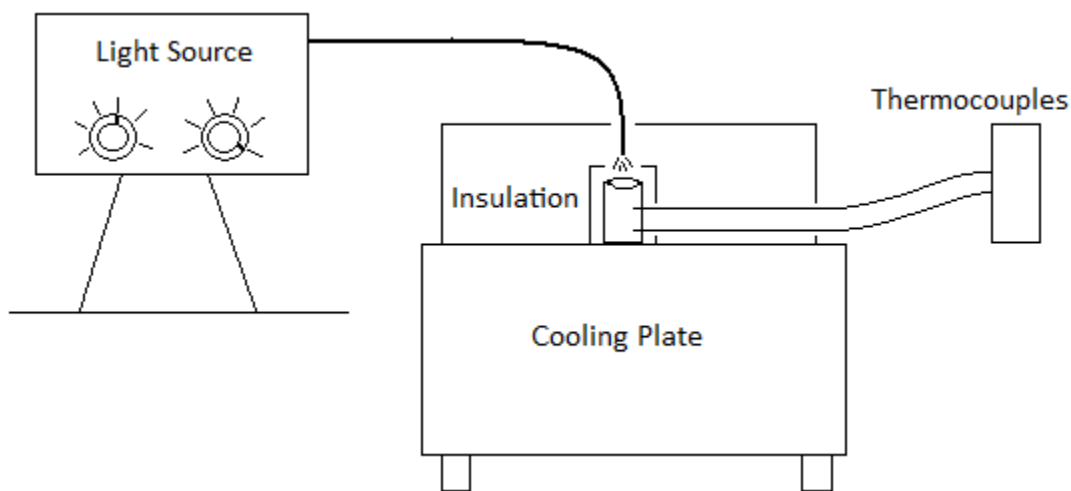


Figure 13. Diagram of the cooling plate setup.

4.2.3 IR camera experiments

The next set of experiments was performed in order to see if the block copolymer was capable of accelerating the melting of ice through its photothermal effect. This was done by freezing 1 mL of the P3HT-*b*-PEO aqueous solution (10 mg/mL) in a transparent plastic cuvette overnight and then exposing it to the LCD light source while measuring the temperature from above with the IR camera. A diagram of the IR camera setup is shown in Figure 14. The temperature was recorded until steady state was reached. Once again, PEDOT:PSS was used as a comparison and water was used as a control.

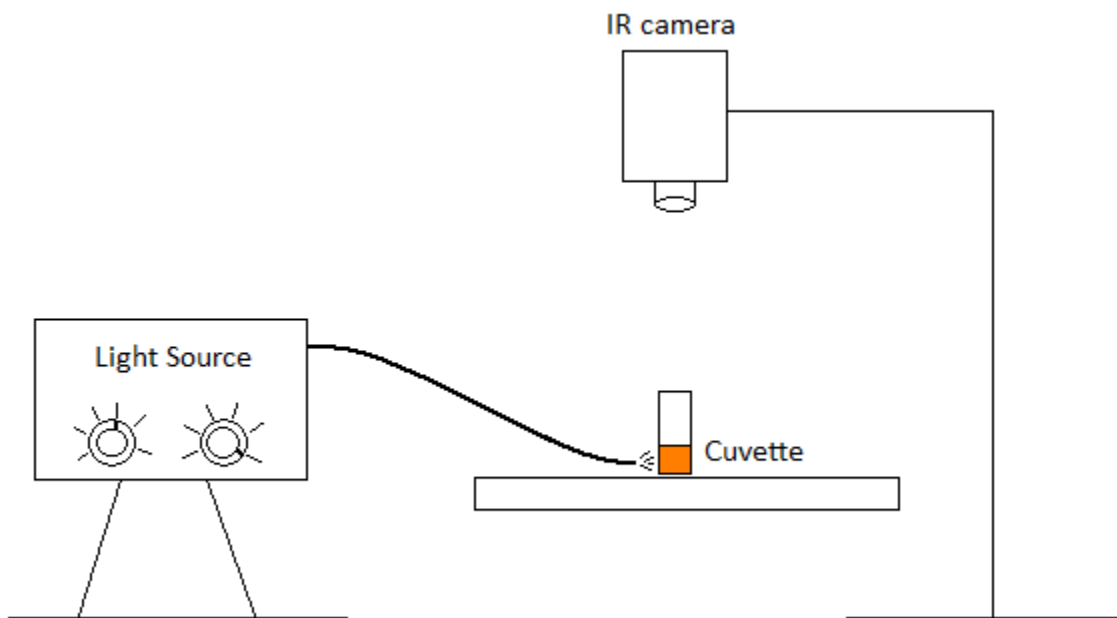


Figure 14. Diagram of the IR camera setup.

4.2.4 Final experiments

The final experiments were performed in order to determine the effect of a different light source and solution colour on solution temperature increase. Similarly to the initial experiments, 1 mL of two P3HT-*b*-PEO aqueous solutions (3 and 10 mg/mL) were put into transparent plastic

cuvettes and exposed to a light source while instantaneous temperature measurements were taken after 5 min, 10 min and 15 min. The diagram of the setup for the final experiments is shown in Figure 11. The only difference between these experiments and the initial experiments is that instead of using the KL 2500 LCD light source, the KL 2500 LED light source was used (50% intensity), which emits less IR radiation. The emission spectrum of the LED light source is shown in Figure 15. Pure water and water with different amounts of food colouring (in order to achieve dark blue and orange colours similar to those of the polymer solutions) were used as controls.

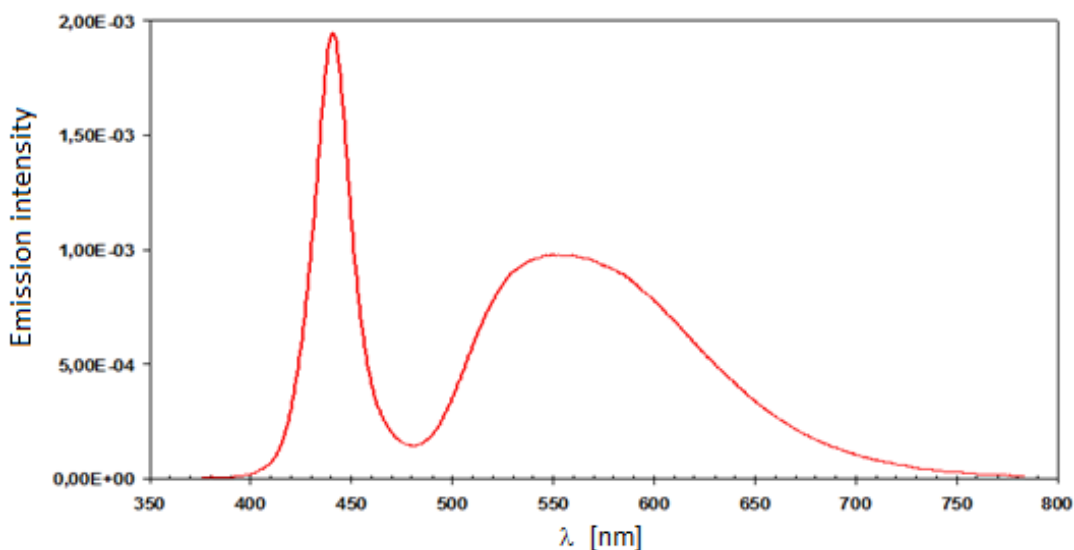


Figure 15. KL 2500 LED light source emission spectrum.

5.0 Results

5.1 Characterization of poly(3-hexylthiophene)

The proton nuclear magnetic resonance (¹H NMR) spectrum in Figure 16 was recorded at ambient temperature on a Varian Mercury-300 spectrometer operating at 300.05 MHz. Chemical shifts are reported in ppm relative to tetramethylsilane (TMS) as an internal standard.

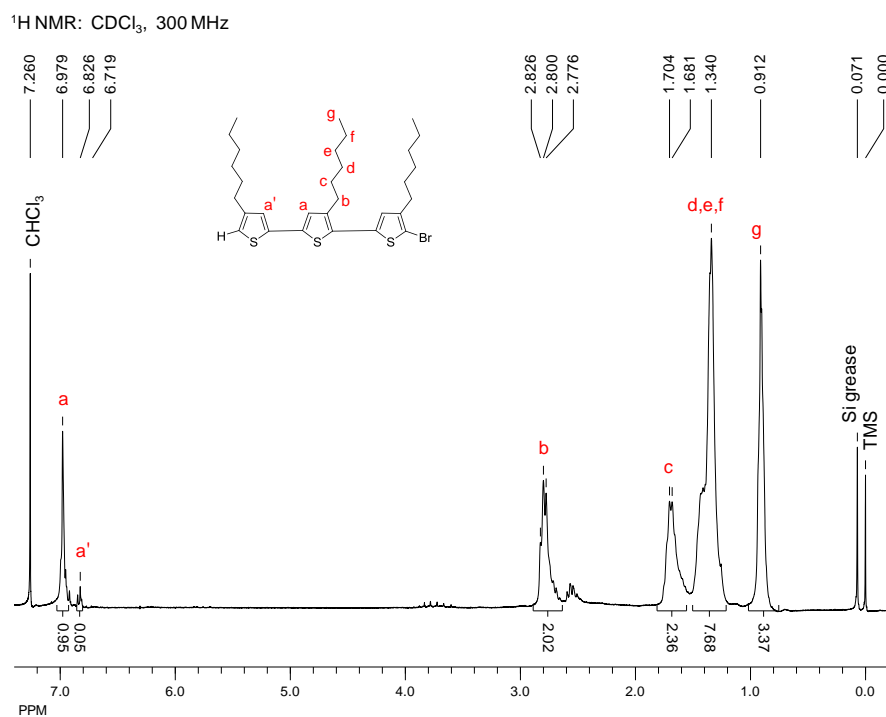


Figure 16. The ¹H NMR spectrum of P3HT.

The ultraviolet-visible absorption spectra for the lower molecular weight P3HT (hexane fraction) and the higher molecular weight P3HT (chloroform fraction) are shown in Figure 17. The maximum absorbance was found to be 437nm and 443nm for the P3HT extracted into hexane and the P3HT extracted into chloroform, respectively. The UV-vis spectra were obtained on the JASCO V-670 spectrophotometer.

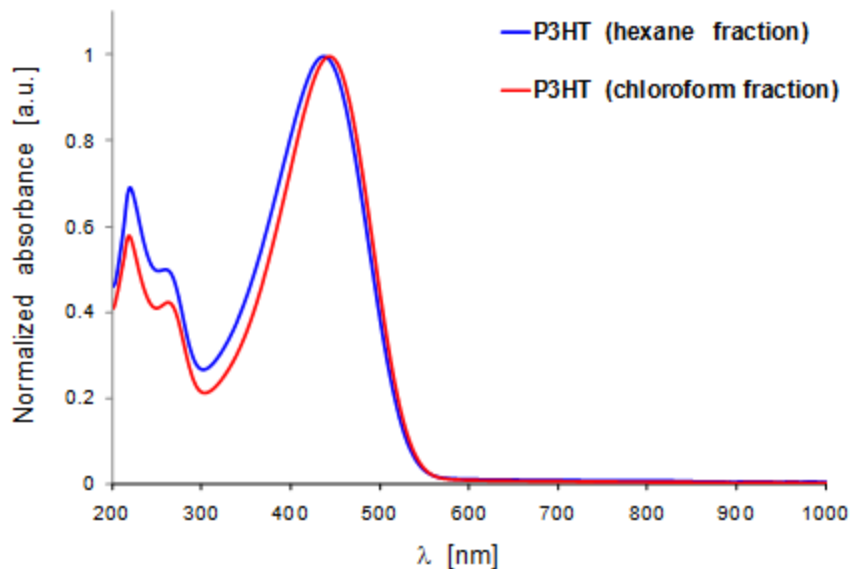


Figure 17. UV-vis absorption spectra of P3HT in THF synthesized using 5% of Ni catalyst.

The matrix assisted laser desorption/ionization-time of flight (MALDI-TOF) mass spectrum of the P3HT extracted into hexane is shown in Figure 18. The higher peaks represent the H,Br-terminated P3HT and the lower peaks represent the H,H-terminated P3HT, as the difference between the peaks corresponds to the difference in the molecular weights of bromine and hydrogen. Therefore, the ratio between the H,H-terminated and H,Br-terminated P3HT is approximately 1:2, since the higher peaks corresponds to approximately double the height of the smaller peaks. The number average molecular weight (M_n) of the P3HT extracted into hexane and used for the synthesis of the P3HT-*b*-PEO block copolymer is about 1700 g/mol according to the MALDI-TOF mass spectrum. The MALDI-TOF mass spectra were obtained on a Bruker Autoflex III MALDI-TOF mass spectrometer using α -cyano-4-hydroxycinnamic acid (HCCA), dithranol (DT), or 2,2':5',2''-terthiophene (TTF) as a matrix.

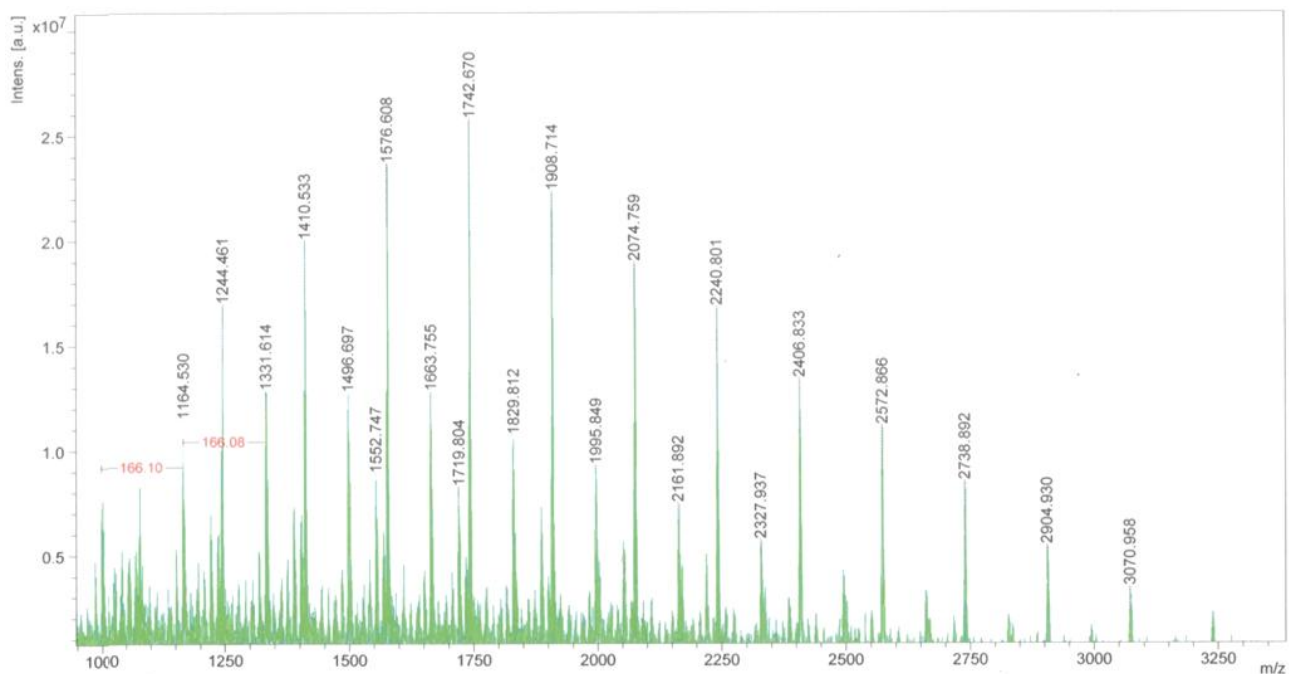


Figure 18. MALDI-TOF mass spectrum of hexane fraction of P3HT synthesized using 2% Ni catalyst and used for P3HT-PEO synthesis.

Gel permeation chromatography (GPC) was performed for the P3HT extracted into hexane and the P3HT extracted into chloroform, shown in Figures 19 and 20 respectively. The M_n of the hexane fraction was found to be about 2400 g/mol and the weight average molecular weight (M_w) was found to be about 2900 g/mol, with a dispersity of 1.2. The M_n of the chloroform fraction was found to be about 9900 g/mol and the M_w was found to be about 14700 g/mol, with a dispersity of 1.48. The GPC measurements were performed on the Varian PL-GPC 50 Plus instrument equipped with UV-vis and IR detectors, using THF as an eluent.

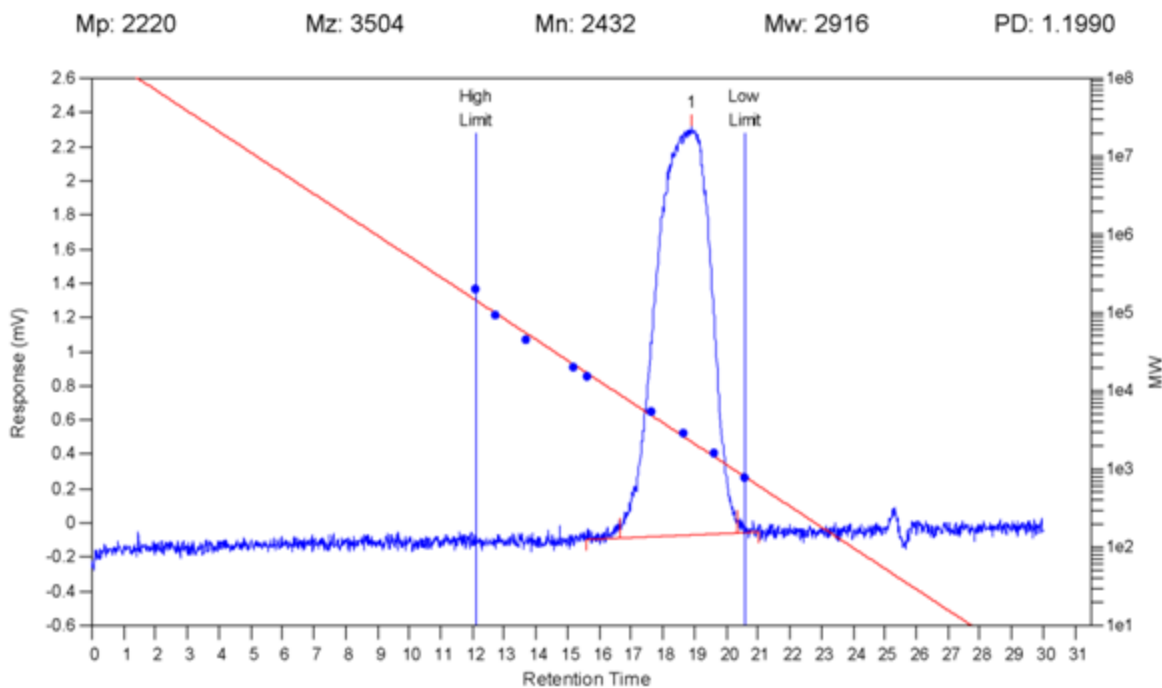


Figure 19. GPC (THF, against polystyrene standard) of the lower molecular weight P3HT extracted with hexane, synthesized using 2% Ni catalyst and used for P3HT-PEO synthesis.

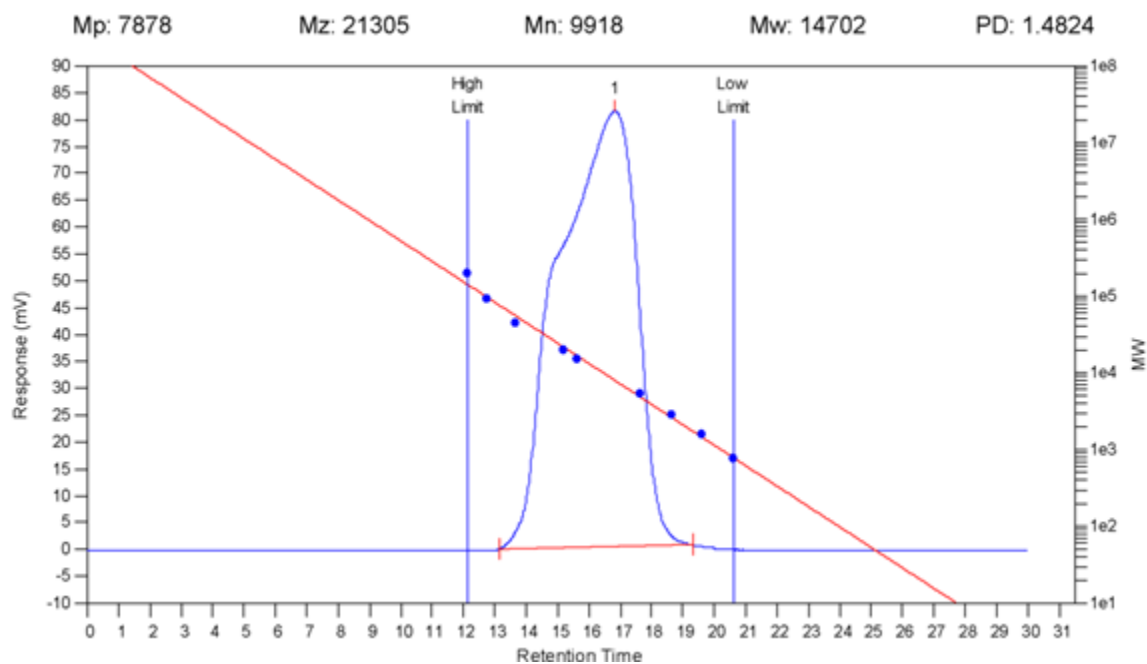


Figure 20. GPC (THF, against polystyrene standard) of the higher molecular weight P3HT extracted with chloroform and synthesized using 2% Ni catalyst.

5.2 Photothermal testing

5.2.1 Initial experiments

Both polymer solutions (PEDOT:PSS and P3HT-PEO) exhibited an increase in temperature upon exposure to the LCD light source in a plastic cuvette, as seen in Figure 21. The PEDOT:PSS solution temperature increased to almost 30°C after 20 minutes and the P3HT-PEO solution increased to almost 25°C, while the temperature increase of the water was negligible (<0.5°C).

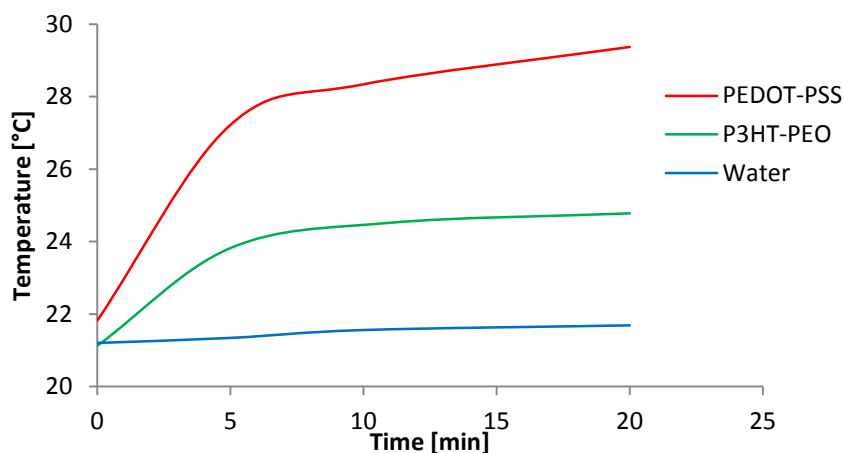


Figure 21. Temperature as a function of time of 1 mL of the three samples in a plastic cuvette exposed to the LCD light source, starting at room temperature.

5.2.2 Cold plate experiments

When using the metal cuvette setup, the two polymer solutions exhibited almost the same temperature increase as water upon exposure to the LCD light source. The temperature of the P3HT-PEO solution is less than 1°C higher than either of the PEDOT:PSS and water solutions at the top thermocouple and just over 1°C higher than the PEDOT:PSS solution at the bottom thermocouple, as seen in Figure 22. The experiments were run until a steady state temperature

was reached. The top thermocouples register higher temperatures than the bottom thermocouples because they are closer to the light source and have more direct exposure.

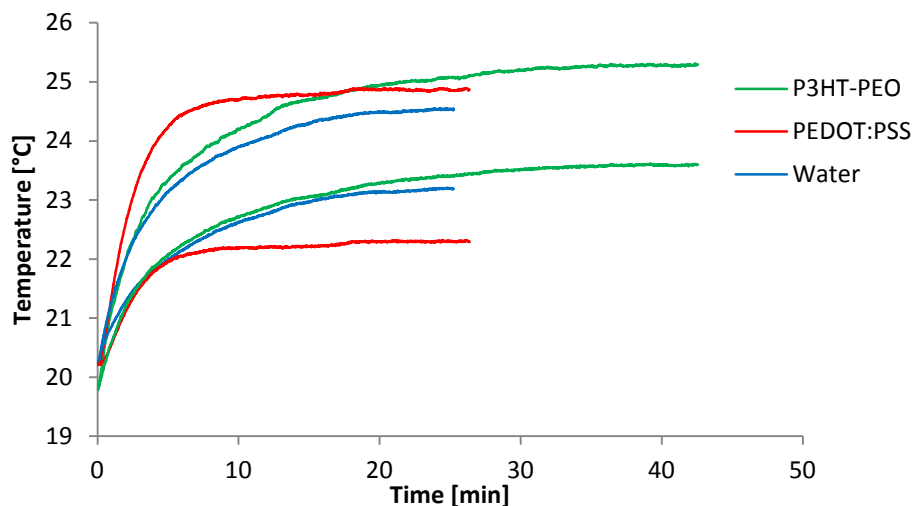


Figure 22. Temperature as a function of time of 2 mL of the three samples in the metal cuvette on the cooling plate exposed to the LCD light source, starting from room temperature.

Figure 23 illustrates the temperature of the three solutions, measured by the top thermocouple, as they are being cooled and frozen on the cooling plate set to -15°C (with the light source off). The P3HT-PEO solution had a different maximum temperature just after nucleation than the other two solutions. The steady state temperature of all three solutions measured by the top thermocouple was the same, approximately -3.8°C .

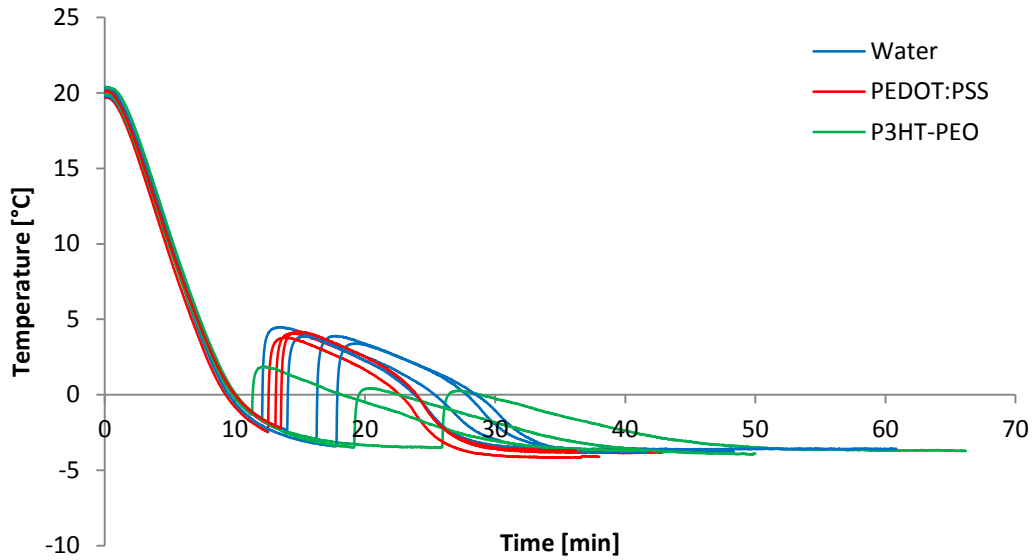


Figure 23. Temperature as a function of time of 2 mL of the three samples in the metal cuvette on the cooling plate set to -15°C starting from room temperature (20°C).

Once the three samples were frozen in the metal cuvette with the cooling plate set at -15°C and then exposed to the LCD light source, the temperature of the ice increased the quickest, as seen in Figure 24. However, the ice did not melt at all. The temperature of the P3HT-PEO sample increased the slowest, but half of it melted, while the rest remained slush. The PEDOT-PSS sample melted a few mm down while the rest was frozen solid.

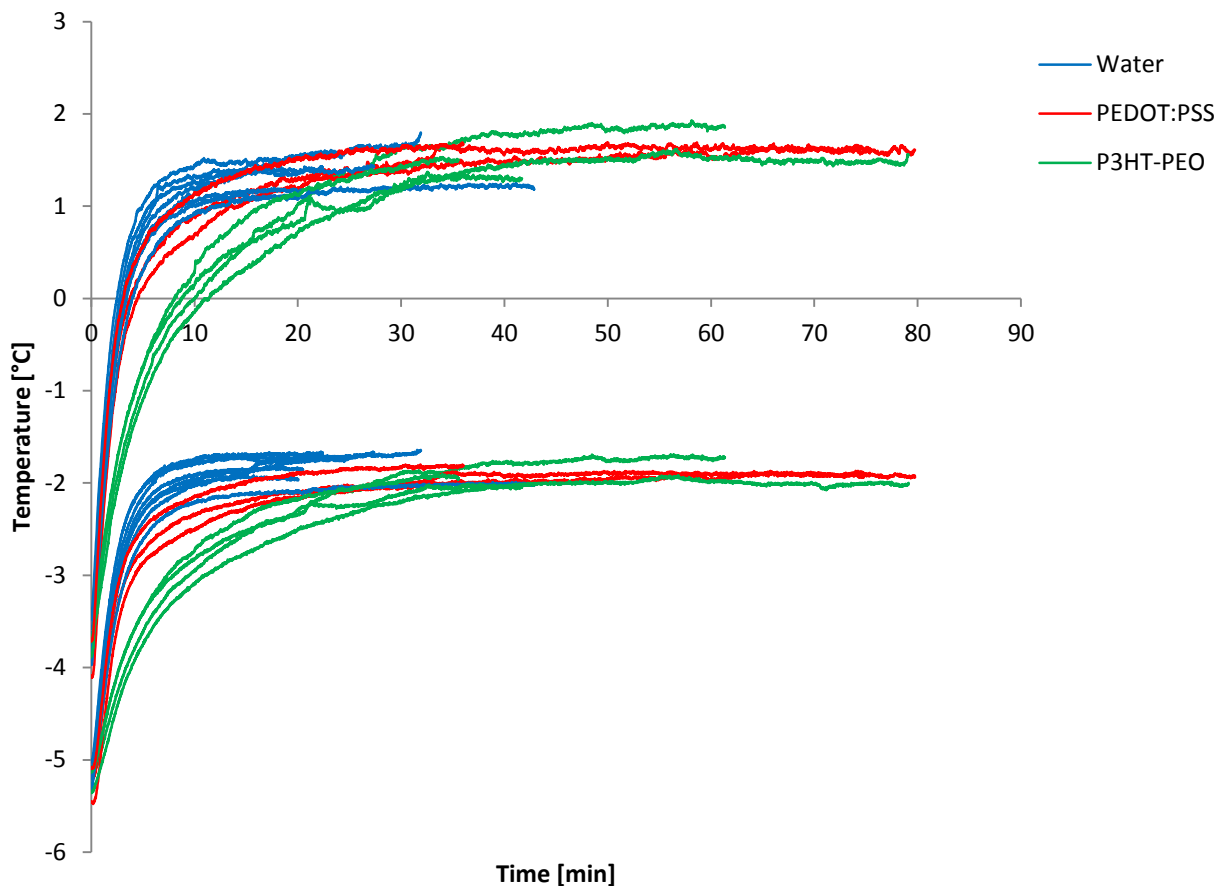


Figure 24. Temperature as a function of time of 2 mL of the three samples exposed to the LCD light source after being frozen in the metal cuvette while the cooling plate was set to -15°C .

When the samples were exposed to the LCD light source at the same time as being cooled by the cooling plate (set to -15°C), none of them froze. The temperature measured by the bottom thermocouple showed no difference between the three samples, as can be seen in Figure 25. However, the temperature of the PEDOT-PSS solution measured by the top thermocouple was the highest, followed by the P3HT-PEO solution, and then water.

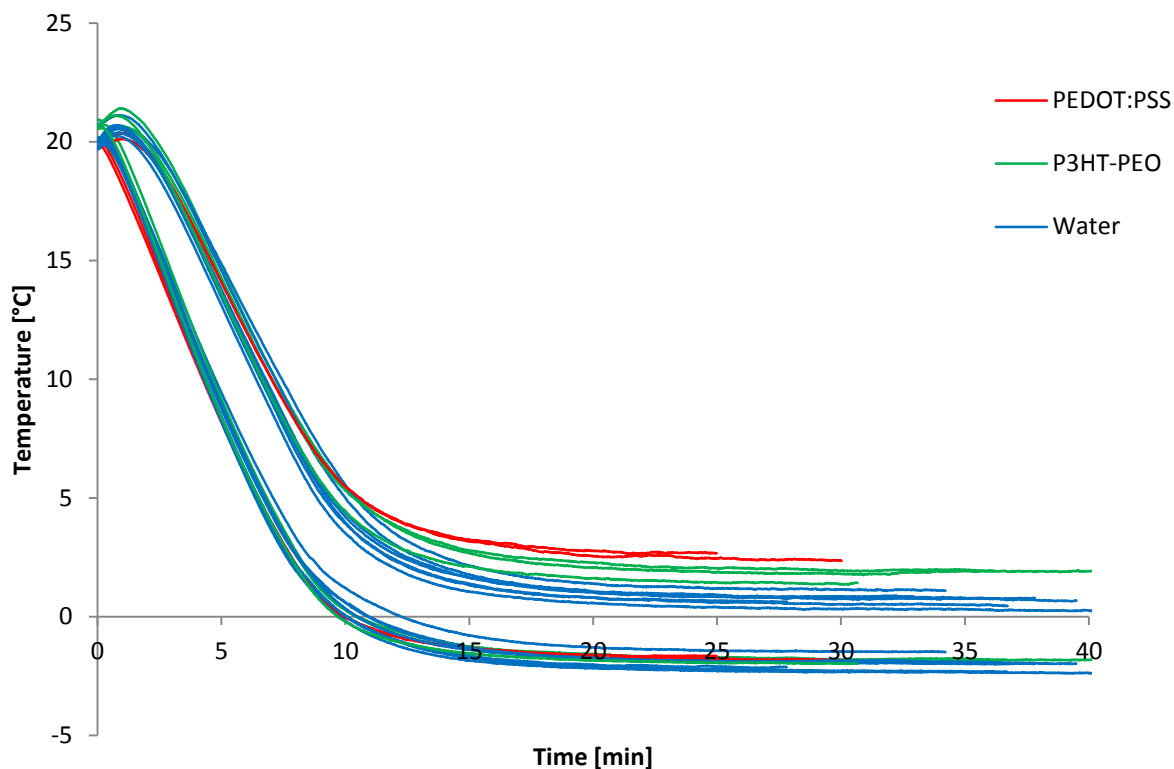


Figure 25. Temperature as a function of time of 2 mL of the three samples in the metal cuvette exposed to the LCD light source while the cooling plate is set at -15°C starting from room temperature.

5.2.3 IR camera experiments

The PEDOT-PSS and ice showed similar initial temperature rises when exposed to the LCD light source in a plastic cuvette. However, the PEDOT-PSS completely melted more quickly than the water and reached steady state at around 40°C , as seen in Figure 26. Even though, the P3HT-PEO sample heated more slowly at the beginning, it completely melted less than five minutes after the PEDOT-PSS. The water took almost 30 minutes to melt completely before reaching steady state less than 1°C above room temperature.

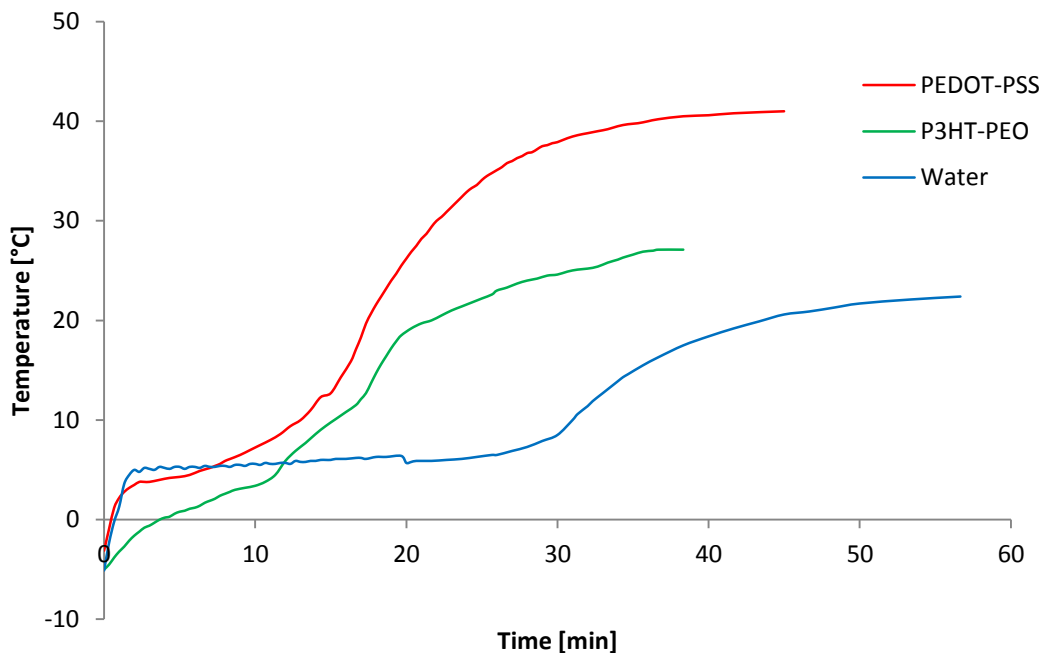


Figure 26. Temperature (measured with an IR camera) as a function of time of 1 mL of the three samples previously frozen in a plastic cuvette and exposed to the LCD light source.

5.2.4 Final experiments

The water without food colouring did not increase in temperature upon exposure to the LED light source, as shown in Figure 27. The 10 mg/mL P3HT-PEO solution (orange in colour) increased to 38°C while the 3 mg/mL solution (pale orange in colour) increased to 30°C. The water with orange food colouring showed a very similar increase in temperature as the 10 mg/mL P3HT-PEO solution. Finally, the water with dark blue food colouring exhibited the greatest increase in temperature after 15 minutes, reaching a temperature of 42°C.

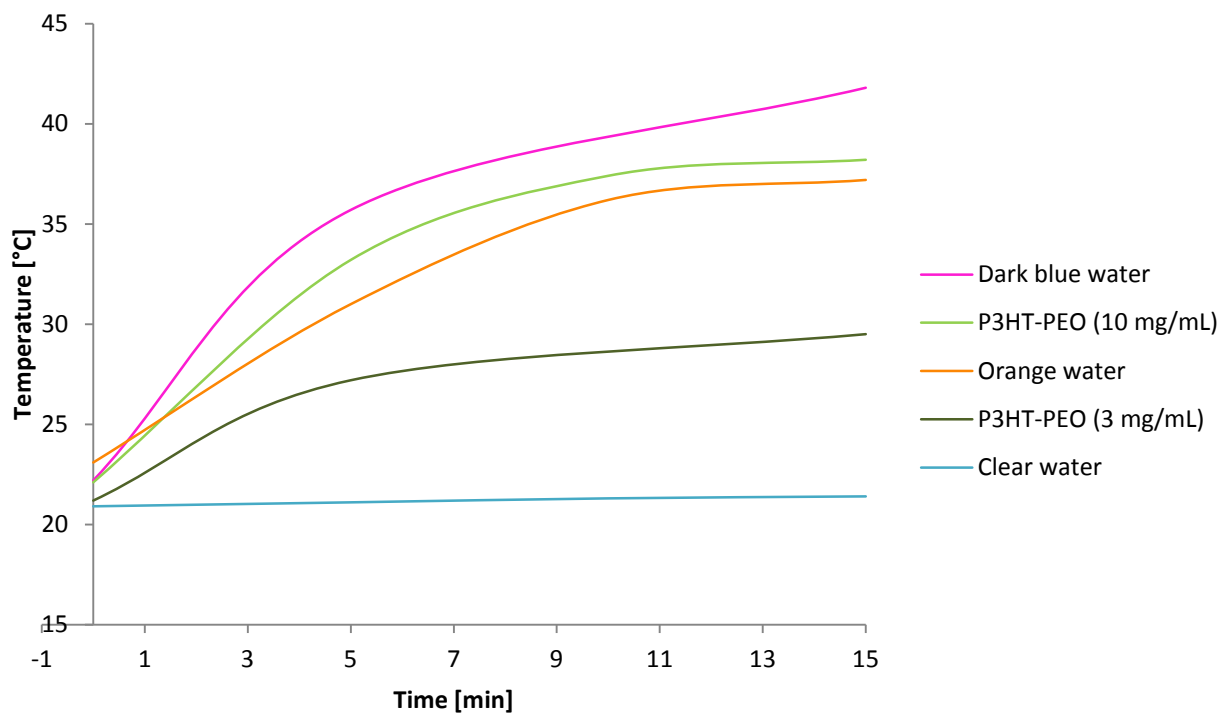


Figure 27. Temperature as a function of time of 1 mL of sample in a transparent plastic cuvette exposed to the LED light source, starting from room temperature.

6.0 Discussion

The polymer characterization experiments in section 5.1 confirmed the successful synthesis of regioregular P3HT using the GRIM method. The ¹H NMR spectrum in Figure 16 shows that 3-hexylthiophene was polymerized with approximately 95% head-to-tail coupling (the ratio between a and a' confirms this), making it regioregular. The broad peaks (a to g) are characteristic of a polymer, confirming polymerization. The P3HT had to be regioregular in order to be electrically conductive and hence have photothermal potential.

It was also found that the P3HT-PEO block copolymer was successfully synthesized. The P3HT-PEO was in fact water soluble. The P3HT extracted into hexane (the lower molecular weight P3HT, $M_n = 2400$ g/mol by GPC) was used in the synthesis of the block copolymer along with a high molecular weight PEO ($M_n = 20,000$ g/mol) in order to ensure that the block copolymer would be soluble in water. PEO is soluble in water, but P3HT is not. Therefore, the water soluble portion of the block had to be much larger than the water insoluble portion (mass ratio of about 10:1 was chosen in this case); otherwise the block copolymer could form inverse micelles which would be insoluble in water.

The initial experiments, using a plastic cuvette and LCD light source at room temperature, demonstrated that the P3HT-PEO solution did indeed exhibit photothermal behaviour (increasing by 4°C), but not to the same extent as the PEDOT:PSS solution (increasing by 8°C), as seen in Figure 21. The water, used as a control, did not increase in temperature which suggested that the polymers were in fact the cause of the temperature increase in the other two solutions.

The first cold plate experiment (using a metal cuvette and LCD light source at room temperature) demonstrated that water experienced an equivalent temperature increase to the polymer solutions (seen in Figure 22), contrary to the results obtained in the initial experiments (performed using a plastic cuvette and instantaneous temperature measurements). The explanation for this is twofold. First, the thermocouples themselves are affected by incident light. When exposed directly to the light source (as in the case of the cold plate experiments), the temperature read by the thermocouples increased between 5 and 10°C, depending on the length of exposure. Also, the metal cuvette itself increases in temperature when exposed to the LCD light source. The LCD light source emits not only photons but phonons as well, and the metal absorbs this heat and transfers it to the water. Second, the metal cuvette and the cooling plate on which it rested are both thermally conductive, resulting in faster heat dissipation through the cuvette walls and cold plate. This in turn reduces the effect of the photothermal polymers and therefore reduces the steady state temperature they are able to reach. Furthermore, the bottom thermocouple for the PEDOT-PSS read a noticeably lower temperature most likely because the solution was so dark that the light could not penetrate to the bottom and therefore only heated the top while heat was being transferred out from the bottom of the cuvette to the cooling plate.

The quantitative results obtained in the second cold plate experiment, which involved exposing the frozen samples (cooling plate set at -15°C) to the LCD light source in the metal cuvette, suggested no difference in the photothermal behaviour of water and the two polymer solutions, contrary to what was previously found with the plastic cuvette. The steady state temperature of each of the three samples after turning on the light was about the same as seen in Figure 24 (1.5°C top thermocouple, -2°C bottom thermocouple), due to the effect of the LCD light source on the thermocouples mentioned above. Also, the temperature of the ice increased

the quickest due to the fact that the thermocouples are affected by incident light, and since ice is clear unlike the two polymer solutions, it receives more incident light. However, the ice did not melt. Despite having the same temperature as the ice, the PEDOT:PSS sample melted a few millimetres at the top, but remained frozen at the bottom. Despite being the slowest to rise in temperature, the P3HT-PEO sample melted halfway down, while the bottom half was slush. The slower rise in temperature is probably due to the fact that the P3HT-PEO sample was melting the most and melting is an endothermic process. These qualitative observations would suggest that the presence of these photothermal polymers in water did in fact help melt the ice, especially in the case of the P3HT-PEO. It could also mean that the polymers affect the melting temperature of the ice.

In the third cold plate experiment, which involved exposing the samples in the metal cuvette to the light source while cooling (cooling plate was set to -15°C), the LCD light source had such a great effect on the metal cuvette that none of the solutions managed to freeze, as seen in Figure 25. Therefore, it was unable to be determined whether or not having the photothermal polymers in solution helped prevent the water from freezing. The top thermocouple did show higher temperatures for the two polymer solutions indicating a photothermal effect.

In the IR camera experiments, the IR camera only measured the temperature at the surface of the solutions in the plastic cuvettes. The temperature at the top of the solutions increased quickly as the solutions melted, seen in Figure 26. However, once the remaining ice detached from the wall, it floated to the top, skewing the temperature measurement. Therefore, as long as the temperature stayed relatively constant as seen in Figure 26 (whether it may be at 0°C or not), it meant that the solutions had not completely melted. The P3HT-PEO and PEDOT:PSS solutions had very small constant temperature portions, compared to water, indicating that once

the solution started to melt, it melted quickly. This may be due to the fact that as a liquid the photothermal behaviour of these solutions is much greater than as solids. This could also explain why PEDOT:PSS and water had similar initial rates of temperature increase. Therefore, these results would suggest that the presence of these polymers in water did help melt the ice faster.

In the final experiments (using a plastic cuvette), an LED light source was used instead of an LCD light source. The LED light source has a maximum emission wavelength of 440 nm, corresponding almost exactly to the maximum absorbance of the P3HT (437 nm). This explains why the temperature of the P3HT-PEO solutions exposed to the LED light source increased more than when exposed to the LCD light source (in the initial experiments), which has a maximum emission wavelength of 670 nm.

However, after the addition of food colouring, one of the coloured water samples (orange) exhibited approximately the same increase in temperature as P3HT-PEO, while another (dark blue) exhibited a greater increase in temperature than the 10 mg/mL P3HT-PEO solution upon exposure to the LED light source, as seen in Figure 27. The darker the solution, the higher the temperature increase was. Therefore, perhaps the extent of the previously observed photothermal behaviour was simply a result of how dark the solutions were and not actually due to the photothermal effect of the polymers.

7.0 Conclusion

In conclusion, a P3HT-PEO block copolymer was successfully synthesized and solubilised in water. Upon exposure to the light source, the P3HT-PEO solution increased in temperature unlike the water control, suggesting photothermal conversion of light to heat. The PEDOT:PSS polymer solution used as a comparison showed greater photothermal efficiency than P3HT-PEO. The interactions between the light source and the thermocouples and metal cuvette proved to have a large impact on the results obtained with the cooling plate setup. The photothermal effect of the polymers, when compared to water, was greatly reduced with this setup. The data collected did not permit the determination of whether the photothermal polymers could prevent or delay the water from freezing upon exposure to the light source under a constant cooling load (-15°C). However, the presence of the polymers in water appeared to help melt ice upon exposure to the light source under a constant cooling load (-15°C), as the frozen polymer solutions partially melted while the water sample remained completely frozen. In this case, the P3HT-PEO sample melted more than the PEDOT:PSS sample.

Furthermore, when exposed to the light source, at room temperature with no cooling, the previously frozen aqueous polymer solutions (P3HT-PEO and PEDOT:PSS) melted faster than just ice, meaning that the photothermal effect of these polymers helped quicken the melting process.

The LED light source was more effective than the LCD light source, as it had an emission spectrum more similar to the absorption spectrum of P3HT-PEO. Consequently, the P3HT-PEO solution demonstrated a greater increase in temperature when exposed to the LED light source compared to the LCD light source (17°C compared to 4°C). However, the dark

coloured water experienced the same increase in temperature as the P3HT-PEO samples, while the clear water had no change. The amount of temperature increase was found to depend on the (colour) darkness of the solution. This puts into question the photothermal effect of the polymers or suggests a potential photothermal behaviour exhibited by the food colouring.

7.1 Recommendations

Due to the colour effect, it would be useful to redo the experiments using dark coloured water instead of pure water. Furthermore, in the cooling plate experiments, the cooling load could be increased in order for the pure water sample to freeze even upon exposure to the light. This would then be more likely to show whether the photothermal polymers could actually help prevent the water from freezing. A more accurate way to measure the temperature of the water and ice that is not affected by the light source would also be beneficial. If these new experiments were to show promising results, further experiments using a hydrate forming chemical such as THF, instead of just water, would be the next step in determining the effectiveness of photothermal polymers in hydrate inhibition.

8.0 References

1. Sloan, E.D. and C.A. Koh, *Clathrate hydrates of natural gases*. 3rd ed. Chemical industries. 2008, Boca Raton, FL: CRC Press. xxv, 721 p., 8 p. of plates.
2. Chatti, I., et al., *Benefits and drawbacks of clathrate hydrates: a review of their areas of interest*. *Energy Conversion and Management*, 2005(46): p. 1333-1343.
3. Hessel, C.M., et al., *Copper selenide nanocrystals for photothermal therapy*. *Nano Lett*, 2011. **11**(6): p. 2560-6.
4. Lee, C., et al., *Porous silicon as an agent for cancer thermotherapy based on near-infrared light irradiation*. *J. Mater. Chem.*, 2008(18): p. 4790-4795.
5. Maity, S., J.R. Bochinski, and L.I. Clarke, *Metal Nanoparticles Acting as Light-Activated Heating Elements within Composite Materials*. *Advanced Functional Materials*, 2012. **22**(24): p. 5259–5270.
6. Robinson, J.T., et al., *Ultrasmall reduced graphene oxide with high near-infrared absorbance for photothermal therapy*. *J Am Chem Soc*, 2011. **133**(17): p. 6825-31.
7. Cheng, L., et al., *Organic stealth nanoparticles for highly effective in vivo near-infrared photothermal therapy of cancer*. *ACS Nano*, 2012. **6**(6): p. 5605-13.
8. Institute of Petroleum Engineering, H.-W.U. *Where are Gas Hydrates Found?* January 8, 2013]; Available from: http://www.pet.hw.ac.uk/research/hydrate/hydrates_where.cfm?hy=what
9. Bai, Y., *Subsea Pipelines and Risers*. 2005, Kidlington, Oxford: Elsevier Inc.
10. Saldívar-Guerra, E. and E. Vivaldo-Lima, *Handbook of polymer synthesis, characterization, and processing*. xxi, 622 pages.
11. Avadhanulu, N., *A Textbook Of Engineering Physics For B.E., B.Sc. (Engg.)*. 1992: S Chand & Company.
12. Brédas, J.L. and G.B. Street, *Polarons, Bipolarons, and Solitons in Conducting Polymers*. *Acc. Chem. Res.*, 1985. **18**: p. 309-315.
13. Minges, M.L. and A.S.M.I.H. Committee, *Electronic Materials Handbook: Packaging*. 1989: Taylor & Francis.
14. Kotz, J.C., P. Treichel, and J.R. Townsend, *Chemistry & chemical reactivity*. 8th ed. 2012, Belmont, CA: Brooks/Cole, Cengage Learning. xxxii, 1093, 132, 29 p.
15. Martin, P., *Introduction to Surface Engineering and Functionally Engineered Materials*. 2011: Wiley.
16. Debashis, D., *Basic Electronics*. 2010: Dorling Kindersley.

17. Kakani, S.L. and K.C. Bhandari, *Electronics Theory and Applications*. 4th ed. 2011, New Delhi, India: New Age International Ltd.
18. Rajendran, V., *Materials Science*. 2004, Tata McGraw-Hill Publishing Company Ltd.: New Delhi, India.
19. Scrosati, B., *Applications of electroactive polymers*. 1st ed. 1993, London ; New York: Chapman & Hall. xiii, 354 p.
20. MacNeill, C.M., et al., *Low band gap donor-acceptor conjugated polymer nanoparticles and their NIR-mediated thermal ablation of cancer cells*. *Macromol Biosci*, 2013. **13**(1): p. 28-34.
21. Di, B., et al., *Formation and evolution dynamics of bipolarons in conjugated polymers*. *J Phys Chem B*, 2011. **115**(5): p. 964-71.
22. Loewe, R.S., et al., *Regioregular, Head-to-Tail Coupled Poly(3-alkylthiophenes) Made Easy by the GRIM Method: Investigation of the Reaction and the Origin of Regioselectivity*. *Macromolecules*, 2001. **34**: p. 4324-4333.
23. Perepichka, I., *Synthesis of P3HT-PEO diblock copolymer*. 2013, McGill University.
24. Li, F., et al., *Fine dispersion and self-assembly of ZnO nanoparticles driven by P3HT-b-PEO diblocks for improvement of hybrid solar cells performance*. *New J.Chem.*, 2013. **37**: p. 195-203.

Appendix

A-1 Characterization of P3HT synthesized using 5% nickel catalyst

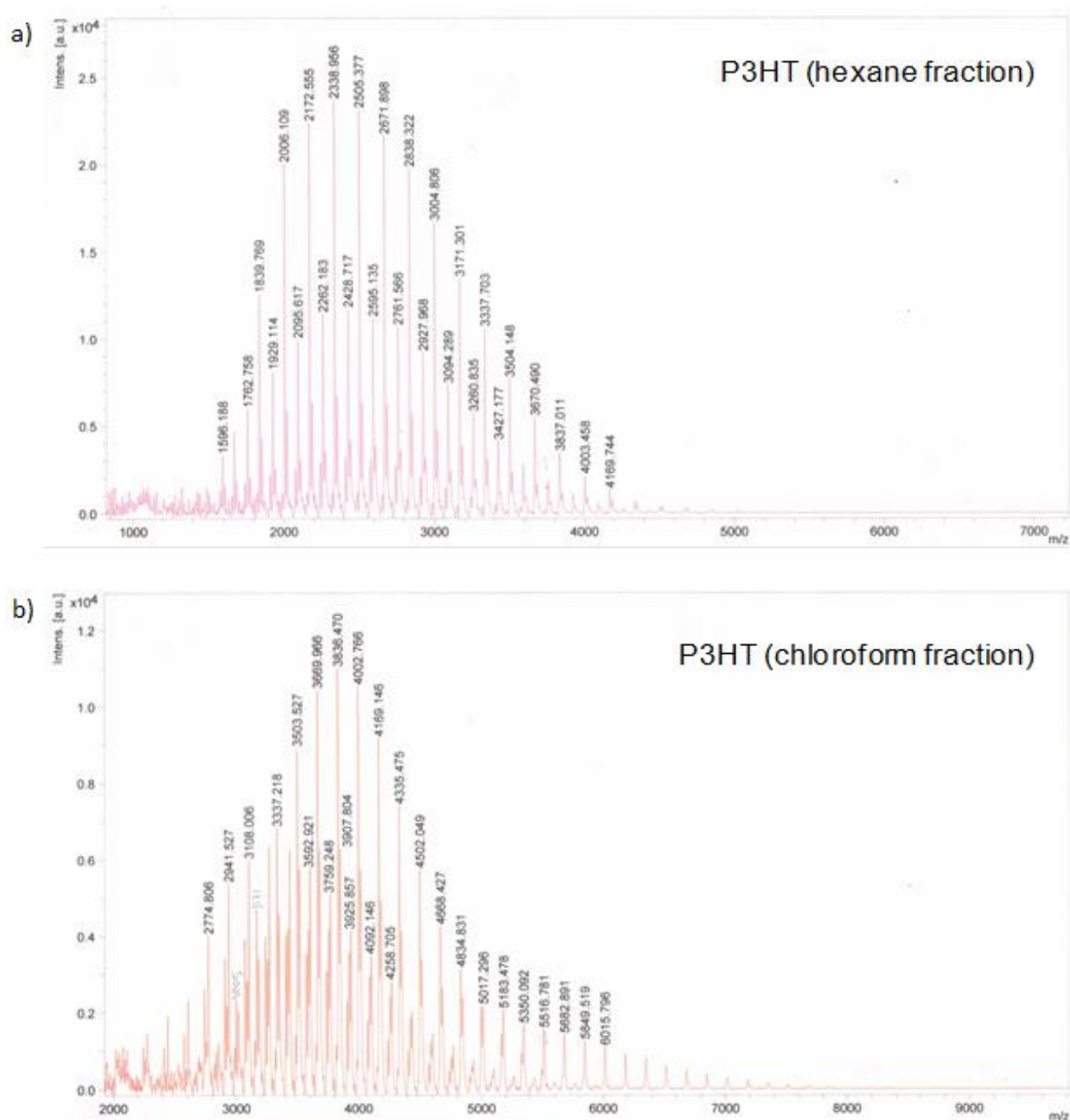


Figure 28. MALDI-TOF mass spectra of P3HT synthesized using 5% nickel catalyst. a) lower molecular weight fraction (P3HT extracted with hexane). b) higher molecular weight fraction (P3HT extracted with chloroform).

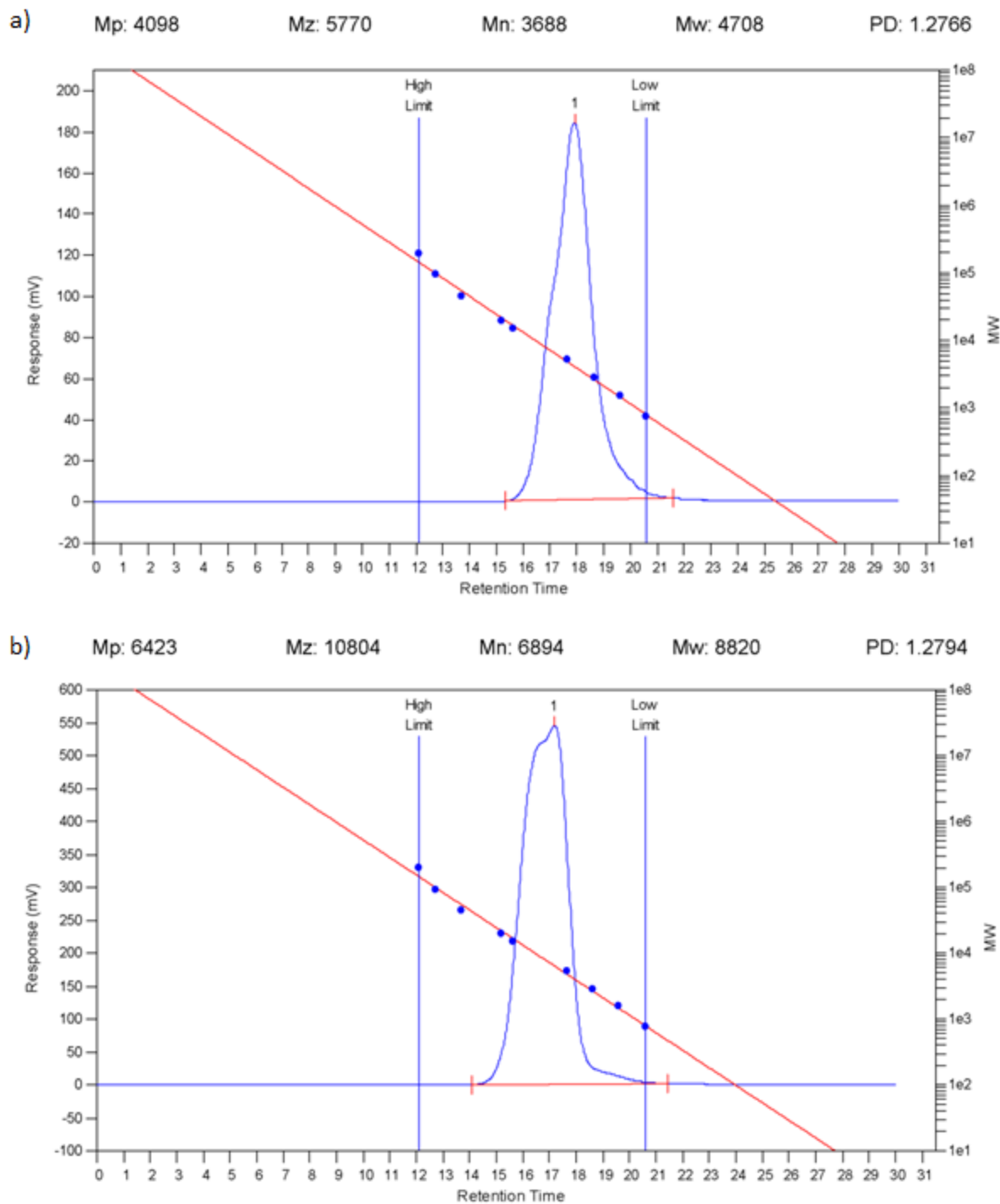


Figure 29. GPC (THF, UV detection at 440 nm, polystyrene standard) of P3HT synthesized using 5% nickel catalyst. a) lower molecular weight fraction (P3HT extracted with hexane). b) higher molecular weight fraction (P3HT extracted with CHCl_3).